Neutralino production as a SUSY discovery process at CERN LEP 2

Sandro Ambrosanio* and Barbara Mele†
Dipartimento di Fisica, Università "La Sapienza" and INFN, Sezione di Roma, P.le Aldo Moro 2, I-00185 Rome, Italy
(Received 17 March 1995; revised manuscript received 21 June 1995)

A thorough study is performed on pair production and signatures of supersymmetric neutralinos in the MSSM at LEP 2. Particular attention is paid to the region of the SUSY parameter space where the associated production of lightest and next-to-lightest neutralinos is the only visible allowed supersymmetric process. In that region, the signal is critically dependent on the selectron masses $m_{\tilde{e}_{L,R}}$. For $\sqrt{s}/2 < m_{\tilde{e}_{L,R}} \lesssim 200$–$300$ GeV and charginos above the threshold for pair production, neutralinos arising from $e^+e^- \to \tilde{\chi}_1^0\tilde{\chi}_2^0$ could be the only SUSY signal detectable at LEP 2.

PACS number(s): 14.80.Ly, 12.60.Jv

I. INTRODUCTION

If supersymmetry (SUSY) is introduced to solve the naturalness problem encountered when embedding the standard model (SM) in a grand unified theory (GUT), one is forced to assume that superpartner masses are not much larger than the scale of the electroweak (EW) symmetry breaking. In particular, the SUSY partners of the particles that interact only electroweakly should be in the lower range of the SUSY mass spectrum. These particles are more efficiently produced at e^+e^- colliders where there is no large QCD background. The lightest SUSY partners of the EW gauge and Higgs bosons will most probably be the first to be accessible in e^+e^- collisions (see, e.g., Ref. [1]).

We restrict ourselves to the framework of the minimal supersymmetric standard model (MSSM) with universality conditions on soft SUSY-breaking parameters at the GUT scale and R parity unbroken [2,3]. In the most likely scenarios, the lightest SUSY particle, that in the hypothesis of conserved R parity is stable, is the lightest neutralino. In this model, all masses and couplings are set by choosing the values of a finite set of parameters at the GUT scale, usually m_0 (the common scalar mass), $m_{1/2}$ (the common gaugino mass), μ (the SUSY Higgs-boson mixing mass), $\tan\beta$ (the ratio of vacuum expectation values for the two Higgs doublets), and A_0 (the common soft-breaking scalar trilinear coupling). Two further parameters (e.g., m_{A^0}, B_0) are needed to describe the Higgs sector if one does not use relations coming from the requirement that the radiative EW-symmetry breaking takes place at the correct scale.

At the CERN e^+e^- collider LEP 2, one could produce sfermion pairs and/or chargino and neutralino pairs. Charged sfermions and charginos, when allowed by phase space, are the easiest *s*particles to produce, since they are always directly coupled to photon and Z^0 vector bosons. On the other hand, in general, the lightest neutralino states are lighter than charginos and sfermions, but they are linear combinations of neutral gauginos and Higgsinos (hence not coupled to photons) that can decouple also from the Z^0 and consequently have lower production cross sections.

In this paper, we concentrate on neutralino production at LEP 2. We consider with particular attention the regions of SUSY-parameter space where sfermions and charginos are above the pair-production threshold at LEP 2 (i.e., they have masses larger than about M_Z), while the lightest neutralino (LN) and next-to-lightest neutralino (NLN) ($\tilde{\chi}_1^0$ and $\tilde{\chi}_2^0$, respectively) can be produced through the process

$$e^+e^- \to \tilde{\chi}_1^0\tilde{\chi}_2^0. \tag{1.1}$$

A spectacular signature is associated with this channel, where $\tilde{\chi}_1^0$ goes out of the experimental apparatus undetected and the jets of particles coming from the $\tilde{\chi}_2^0$ decay are mostly unbalanced in energy and momentum. We do not consider production of lightest-neutralino pairs ($e^+e^- \to \tilde{\chi}_1^0\tilde{\chi}_1^0$), since it gives rise to an invisible signal at Born level. The process (1.1) has been carefully studied at LEP 1 energies, where the absence of a neutralino signal extends the regions of SUSY parameters excluded by direct search and contributions to the Z^0 width of chargino production [4]. Analogously, we want to study the potential of process (1.1) at LEP 2 to probe regions of the parameter space not covered by chargino searches [we will name these regions neutralino regions (NR's)]. To this aim, we carry out an exhaustive analysis of cross sections and decay rates corresponding to all possible signatures in the MSSM, updating and complementing previous partial studies [5,6]. Some results relative to heavier-neutralino pair production will be also presented, when relevant in the neutralino regions.

The reaction (1.1) proceeds through two mechanisms (cf. Fig. 1): an s-channel Z^0 exchange and a t- (u-) channel (either left or right) selectron exchange. Only Higgsino components of neutralinos (that directly couple to Z^0) have a role in the s channel. On the other hand, in the limit of negligible electron mass only photino and Z-ino components take parts into the t-channel diagrams.

*Electronic address: ambrosanio@roma1.infn.it
†Electronic address: mele@roma1.infn.it

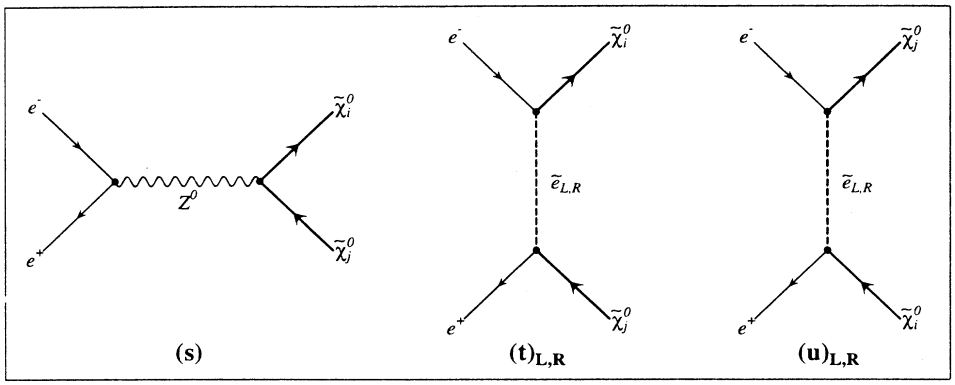

FIG. 1. Feynman diagrams for the process $e^+e^- \to \tilde{\chi}_i^0\tilde{\chi}_j^0$.

At LEP 1, the relevant $\tilde{\chi}_i^0$ components are the Higgsino ones, due to the Z^0 resonance, and cross sections are fixed by only three parameters: M_2, μ, and $\tan\beta$. At LEP 2 the s-channel cross sections in the neutralino regions can be smaller than t-channel ones, and hence the selectron mass becomes a crucial parameter too.

In addition to considering the continuous parameter dependence of our results, some particularly meaningful scenarios will be identified and studied in the neutralino-region parameter space. In Sec. II, we set notations by recalling the neutralino and chargino mass matrices. We also study the physical components and mass spectrum of the two lightest neutralinos as functions of MSSM parameters. Furthermore, we define the neutralino regions and describe their interest. In Sec. III, we study $\tilde{\chi}_1^0\tilde{\chi}_2^0$-production cross sections at LEP 2 and identify a set of significant scenarios for a systematic study. In Sec. IV, some results concerning the main $\tilde{\chi}_2^0$ neutralino decays are reported. A more in-depth investigation on all possible $\tilde{\chi}_2^0$ decay channels can be found in Ref. [7]. Finally, in Sec. V, total rates for all relevant signatures at LEP 2 coming from $\tilde{\chi}_1^0\tilde{\chi}_2^0$ production are studied in detail. In the Appendix, we give formulas that relate scalar masses to the MSSM parameters through renormalization-group equations (RGE's).

II. THE ELECTROWEAK GAUGINO AND HIGGSINO SECTORS

In the MSSM, four fermionic partners of the neutral components of the SM gauge and Higgs bosons are predicted: the photino $\tilde{\gamma}$, the Z-ino $\tilde{Z}$ [mixtures of the U(1) $\tilde{B}$ and SU(2) $\tilde{W}_3$ gauginos], and the two Higgsinos $\tilde{H}_1^0$ and $\tilde{H}_2^0$ (partners of the two Higgs-doublet neutral components). In general, these interaction eigenstates mix, their mixing being controlled by a mass matrix Y [8,9] defined by

$$\mathcal{L}_M^0 = -\frac{1}{2}\psi_i^0 Y_{ij}\psi_j^0 + \text{H.c.}, \tag{2.1a}$$

where

$$Y = \begin{pmatrix} M_2\sin^2\theta_W + M_1\cos^2\theta_W & (M_2 - M_1)\sin\theta_W\cos\theta_W & 0 & 0 \\ (M_2 - M_1)\sin\theta_W\cos\theta_W & M_2\cos^2\theta_W + M_1\sin^2\theta_W & M_Z & 0 \\ 0 & M_Z & \mu\sin 2\beta & -\mu\cos 2\beta \\ 0 & 0 & -\mu\cos 2\beta & -\mu\sin 2\beta \end{pmatrix}. \tag{2.1b}$$

Closely following the notations of Refs. [5,10], Eqs. (2.1) are written by suitably choosing the basis

$$\psi_j^0 = (-i\phi_\gamma, -i\phi_Z, \psi_H^a, \psi_H^b), \quad j = 1,\ldots,4, \tag{2.2}$$

where

$$\psi_H^a = \psi_{H_1}^1\cos\beta - \psi_{H_2}^2\sin\beta\,,$$
$$\psi_H^b = \psi_{H_1}^1\sin\beta + \psi_{H_2}^2\cos\beta\,,$$

and ϕ_γ, ϕ_Z, $\psi_{H_1}^1$, $\psi_{H_2}^2$ are two-component spinorial fields. In Eq. (2.1b), $\tan\beta = \frac{v_2}{v_1}$ and $M_{1,2}$ are the U(1)- and SU(2)-gaugino masses at the EW scale. By assuming gaugino-mass unification at $M_{\rm GUT}$, M_1 can be related to M_2 by the equation

$$M_1 = \frac{5}{3}\tan^2\theta_W M_2, \tag{2.3}$$

that arises from one-loop RGE's (cf. the Appendix). The Y matrix (which, excluding CP violations in this sector of the model, is real and symmetric) can be diagonalized by a unitary 4×4 matrix N:

$$N_{im}N_{kn}Y_{mn} = m_{\tilde{\chi}_i^0}\delta_{ik},$$

where $m_{\tilde{\chi}_i^0}$ $(i = 1,\ldots,4)$ is the mass eigenvalue relative to the ith neutralino state, given by the two-component spinor field $\chi_i^0 = N_{ij}\psi_j^0$. Then, Eq. (2.1a) can be rewritten, by using the four-component neutral Majorana-spinor formalism, in the form

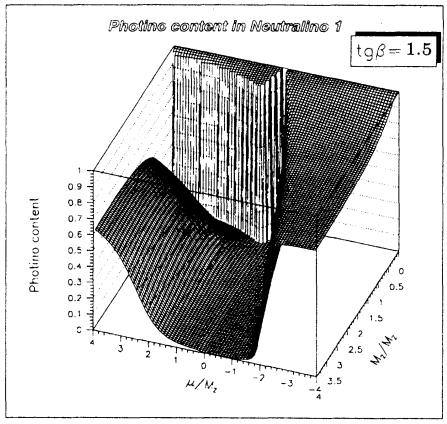

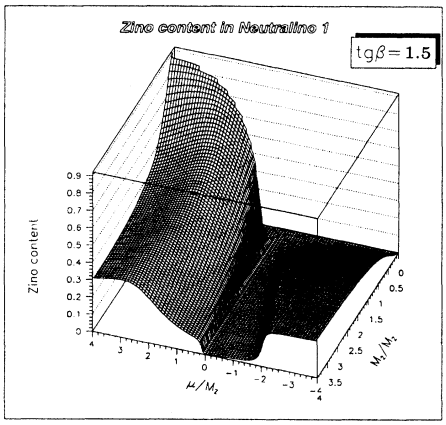

FIG. 2. Photino and Z-ino content in the lightest neutralino vs μ and M_2, for $\tan\beta = 1.5$.

$$\mathcal{L}_M^0 = -\frac{1}{2}\sum_i m_{\tilde{\chi}_i^0}\bar{\tilde{\chi}}_i^0\tilde{\chi}_i^0,$$

where

$$\tilde{\chi}_i^0 = \begin{pmatrix} \chi_i^0 \\ \bar{\chi}_i^0 \end{pmatrix}.$$

The N matrix can be chosen real and orthogonal. In this case some of the $m_{\tilde{\chi}_i^0}$ eigenvalues can be negative. The sign of $m_{\tilde{\chi}_i^0}$ is related to the CP quantum number of the ith neutralino [3,5,11]. By solving a fourth-degree eigenvalue equation, one can find the expressions of $m_{\tilde{\chi}_i^0}$ and of the physical composition of the corresponding eigenstate in terms of the independent parameter set μ, M_2, and $\tan\beta$ (a complete treatment can be found in Ref. [10]).

In our analysis, we study the small and moderate range of $\tan\beta$. This may also be interesting in connection with scenarios with the top quark mass at its infrared fixed point [12]. In particular, we set the value of $\tan\beta$ at either 1.5 or 4. Some results at $\tan\beta = 30$ will also be shown.

Here, we are concerned mainly with the two lightest neutralino states ($i = 1, 2$). In Figs. 2–5, the behavior of their gaugino and Higgsino components (i.e., the square moduli of N_{ij}, for $i = 1, 2$ and $j = 1, \ldots, 4$) is shown for $\tan\beta = 1.5$ versus μ and M_2.

By looking at the Y matrix in Eq. (2.1b), one can easily realize that for either $|\mu| \gg M_Z$ or $M_2 \gg M_Z$ the 2×2 blocks relative to the gaugino and Higgsino sectors do not mix, and the two lightest neutralinos get either both gauginos (with masses close to M_1 and M_2) or both Higgsinos (with degenerate masses close to $\pm|\mu|$).

In Fig. 2, one can note that the photino component of the lightest neutralino is dominant for $M_2 \lesssim M_Z/2$ and $\mu \neq 0$, and in regions where $M_2 \lesssim -2\mu$ with $\mu < 0$, while the $\tilde{Z}$ one is particularly enhanced in the positive-μ half plane for low M_2. Figure 3 shows that the Higgsino components of $\tilde{\chi}_1^0$ are very important in the $2|\mu| \lesssim M_2$ triangle region. In this area, the $\tilde{H}_a^0$ component dominates for $\mu > 0$ and $M_2 \gtrsim M_Z$, whereas the lightest neutralino is nearly a pure $\tilde{H}_b^0$ for $\mu \leq 0$.

The physical composition of $\tilde{\chi}_2^0$ can be observed in Figs. 4 (gauginos) and 5 (Higgsinos). The photino component in $\tilde{\chi}_2^0$ is sizeable only for $2\mu \gtrsim M_2$, if $M_2 \gtrsim M_Z/2$, while a large $\tilde{Z}$ component can be found in the negative-μ half plane for $|\mu| \gg M_2$ or, to a lesser extent, in the positive-μ half plane for M_2 between M_Z and $2M_Z$, provided μ is positive and large enough. Figure 5 shows that the Higgsino composition of the next-to-lightest neutralino is somehow complementary to the lightest neutralino one. The main features of the above pictures remain valid when increasing $\tan\beta$ up to 4.

Concerning the mass spectrum of light neutralinos,

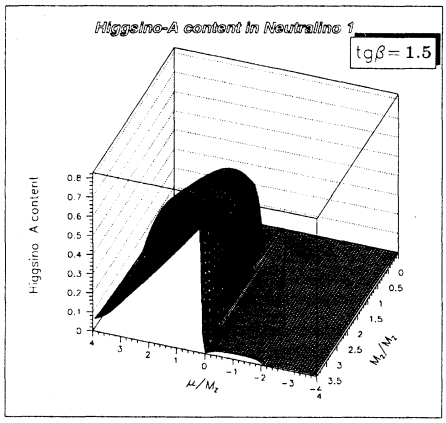

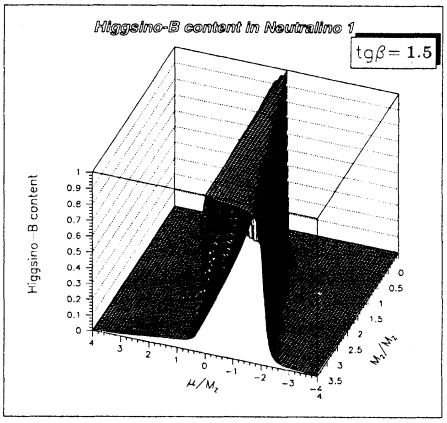

FIG. 3. Higgsino-A and Higgsino-B content in the lightest neutralino vs μ and M_2, for $\tan\beta = 1.5$.

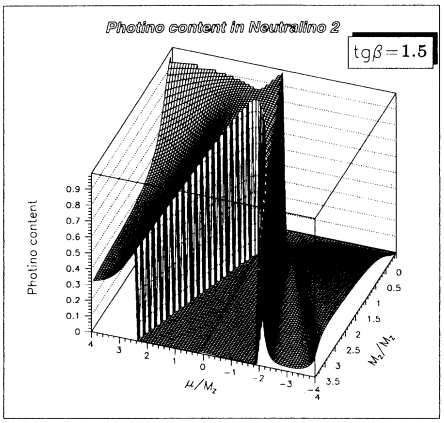

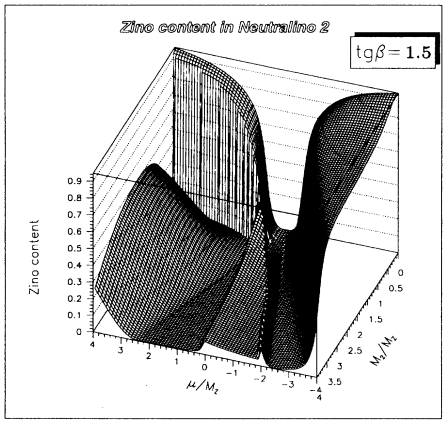

FIG. 4. Photino and Z-ino content in the next-to-lightest neutralino vs μ and M_2, for $\tan\beta = 1.5$.

contour plots for $|m_{\tilde{\chi}_i^0}|$ in GeV are given in Fig. 6 for $\tilde{\chi}_1^0$ and $\tilde{\chi}_2^0$, with $\tan\beta = 1.5$. Dark area represents regions in the (μ, M_2) plane where the mass eigenvalue of the neutralino is negative.

The $m_{\tilde{\chi}_1^0} < 0$ area in Fig. 6 is bounded by the $\mu = 0$ line (along which $\tilde{\chi}_1^0$ is identical to $\tilde{H}_b^0$ and massless), by the hyperbole

$$\mu M_1 M_2 = (M_2 \sin^2\theta_W + M_1 \cos^2\theta_W) M_Z^2 \sin 2\beta \ ,$$

i.e., by using Eq. (2.3), $\mu M_2 = \frac{8}{5} M_W^2 \sin 2\beta$ (along which the $\tilde{\chi}_1^0$ is a massless nontrivial mixed state, mostly made of $\tilde{Z}$ and $\tilde{H}$) and, in the lowest part of the positive-μ half plane, by the contour for crossing of the two lightest neutralino masses that is complementary to the one for $m_{\tilde{\chi}_2^0}$. A similar effect occurs for the $\tilde{\chi}_2^0$-$\tilde{\chi}_3^0$ crossing, as the dark "V" region in the $m_{\tilde{\chi}_2^0}$ contour plot shows. In that region, approximately bounded by the $M_2 = \pm\mu + M_Z$ lines, the Higgsino components dominate both $\tilde{\chi}_1^0$ and $\tilde{\chi}_2^0$. Again, when increasing $\tan\beta$ up to 4, one does not observe substantial variations.

In the following, it will be useful to consider also the chargino sector. The corresponding mass term in the Lagrangian is [3,13]

$$\mathcal{L}_M^{\pm} = -\frac{1}{2}(\psi^+ \ \psi^-) \begin{pmatrix} 0 & X^T \\ X & 0 \end{pmatrix} \begin{pmatrix} \psi^+ \\ \psi^- \end{pmatrix} + \text{H.c.} \ , \quad (2.4a)$$

$$X = \begin{pmatrix} M_2 & M_W\sqrt{2}\sin\beta \\ M_W\sqrt{2}\cos\beta & \mu \end{pmatrix} , \quad (2.4b)$$

where $\psi_j^+ = (-i\phi^+, \ \psi_{H_2}^1)$, $\psi_j^- = (-i\phi^-, \ \psi_{H_1}^2)$, $j = 1, 2$, and $\phi^{\pm}$, $\psi_{H_2}^1$, $\psi_{H_1}^2$ are two-component spinorial fields of W-inos and charged Higgsinos, respectively. The mass matrix X can be diagonalized by two 2×2 unitary matrices U and V:

$$U_{im} V_{jn} X_{mn} = m_{\tilde{\chi}_i^{\pm}} \delta_{ij},$$

where $m_{\tilde{\chi}_i^{\pm}}$ is the mass eigenvalue for the ith chargino state, which is defined by $\chi_i^+ = V_{ij}\psi_j^+$, $\chi_i^- = U_{ij}\psi_j^-$, $i, j = 1, 2$ (V and U are taken to be real after assuming CP conservation). Here $\chi_i^{+(-)}$ are the two-component spinors corresponding to the positive- (negative-)charged part of the four-component Dirac-spinor of $\tilde{\chi}_i^{\pm}$. After diagonalization, one is able to derive a simple formula for the chargino-mass eigenvalues:

$$m_{\tilde{\chi}_{1,2}^{\pm}} = \frac{1}{2}\Big[\sqrt{(M_2 - \mu)^2 + 2M_W^2(1 + \sin 2\beta)} \mp \sqrt{(M_2 + \mu)^2 + 2M_W^2(1 - \sin 2\beta)}\Big] . \quad (2.5)$$

At this point, it is straightforward to set regions in the

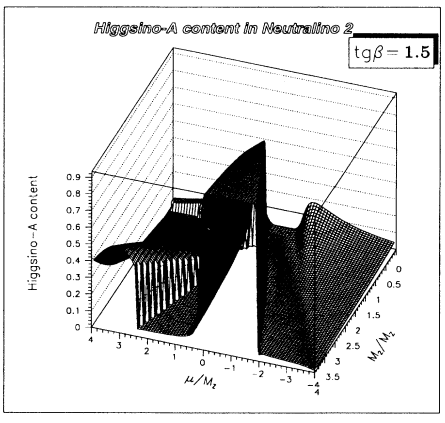

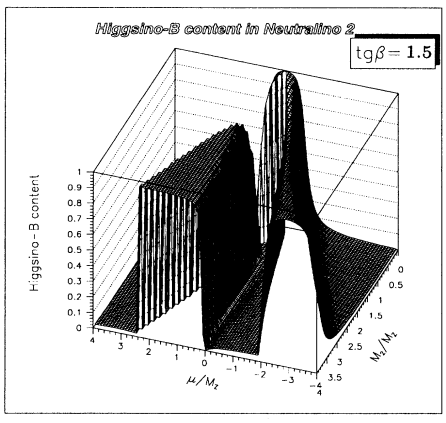

FIG. 5. Higgsino-A and Higgsino-B content in the next-to-lightest neutralino vs μ and M_2, for $\tan\beta = 1.5$.

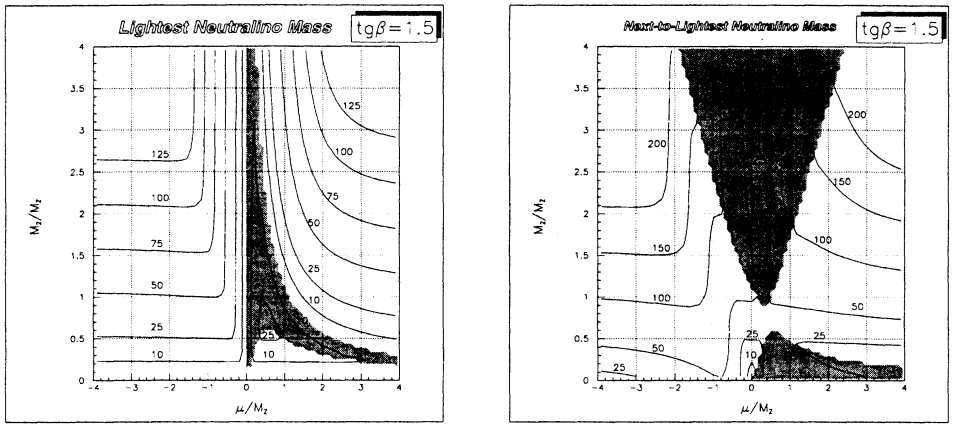

FIG. 6. Contour plot for the modulus of the LN and NLN mass eigenvalues (in GeV) in the (μ, M_2) plane for $\tan\beta$ =1.5. The dark area corresponds to regions where the $\tilde{\chi}^0_{1,2}$-mass eigenvalue is negative.

(μ, M_2) plane, where $\tilde{\chi}^0_1\tilde{\chi}^0_2$ production is allowed by phase space, but chargino-pair production is not, for which one has

$$m_{\tilde{\chi}^0_1} + m_{\tilde{\chi}^0_2} < \sqrt{s} < 2m_{\tilde{\chi}^\pm_1}. \tag{2.6}$$

These regions are shown in Figs. 7 and 8 for $\tan\beta$ = 1.5, 4 and $\sqrt{s}$ = 190 GeV (curves "N190" correspond to $\sqrt{s} = m_{\tilde{\chi}^0_1} + m_{\tilde{\chi}^0_2}$, while curves "$C$190" are for $\sqrt{s} = 2m_{\tilde{\chi}^\pm_1}$). We will call NR$^\pm$ the two disconnected regions where Eq. (2.6) holds and $\mu \gtrless 0$. We can see that there is a conspicuous increase in the accessible parameter space because of the lower neutralino $\tilde{\chi}^0_1 + \tilde{\chi}^0_2$ threshold with respect to chargino pairs. The relevant portions of space are placed, for our choice of $\tan\beta$ values, where $\mu \lesssim -M_Z$ and $\mu \gtrsim 1.5M_Z$. For $\tan\beta$ = 1.5 (Fig. 7), the NR$^-$ is centered around $M_2 = 1.1M_Z$, while the NR$^+$ is slightly shifted to higher M_2 values. By increasing $\tan\beta$ (Fig. 8), the asymmetry in the two regions decreases. The shaded area shows the region excluded by LEP 1.

We do not consider in this work the small modifications of the above general scenario that could arise from radiative corrections to gaugino-Higgsino masses. Recent calculations [14,15] at the one-loop level give indication for typical corrections of the order of 6% (or somewhat higher in particular cases for the lightest neutralino) with the same sign for all neutralino and chargino states. So, they do not change the relative configuration of neutralino and chargino masses and do not affect our general discussion. Also, such corrections are of the same

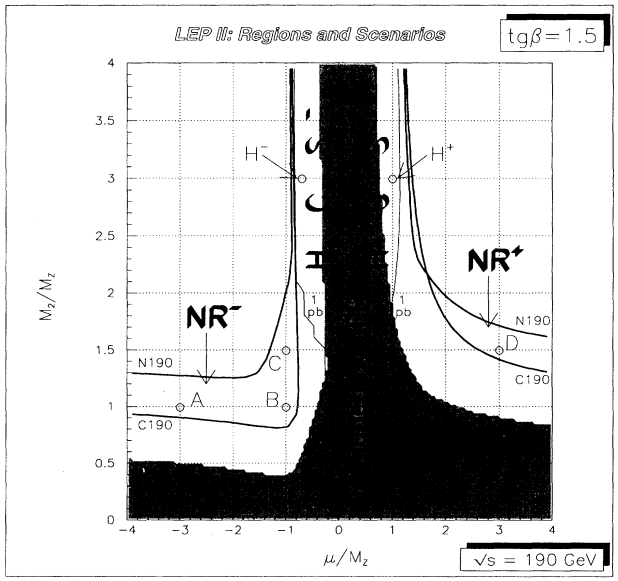

FIG. 7. Interesting regions and scenarios in the (μ, M_2) plane with $\tan\beta$ = 1.5 for neutralino search at LEP 2 ($\sqrt{s}$ = 190 GeV). The NR$^\pm$ regions (bounded by kinematic-limit curves "N190" and "C190" for $\tilde{\chi}^0_1\tilde{\chi}^0_2$ and $\tilde{\chi}^+_1\tilde{\chi}^-_1$ production, respectively) and HCS$^\pm$ regions (outlined by the 1-pb contour plot for the $\tilde{\chi}^0_1\tilde{\chi}^0_2$ total cross section, for $m_0 = M_Z$) are indicated. The shaded area corresponds to LEP 1 limits. The points A–D in NR and $H^\pm$ in HCS will be used in the following analysis.

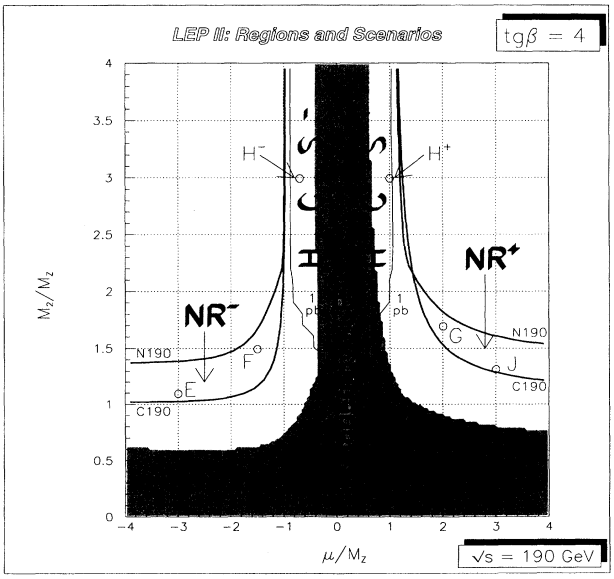

FIG. 8. The same as in Fig. 7 but with $\tan\beta$ = 4. In NR$^\pm$ different points are chosen (E,F,G,J) with respect to the $\tan\beta$ = 1.5 case.

order of magnitude as other neglected effects, e.g., other threshold effects in the RGE evolution.

III. NEUTRALINO CROSS SECTIONS AT LEP 2

In this section, we study the total cross section for the process $e^+e^- \to \tilde{\chi}_1^0\tilde{\chi}_2^0$ at LEP 2. The relevant formulas needed to compute neutralino total cross sections can be found in Ref. [5]. Crucial parameters in the prediction of total rates are the values of selectron masses $m_{\tilde{e}_{L,R}}$ that enter the t-channel amplitudes. These are directly related to m_0 through the RGE's that govern the running of scalar masses from the GUT scale down to M_Z (see the Appendix). Then, one can compute rates for different signals coming from the $\tilde{\chi}_2^0$ decay as functions of m_0, since, once m_0 is fixed, all other scalar particles entering the $\tilde{\chi}_2^0$ decays (excluding Higgs bosons) are set too, for any M_2 and $\tan\beta$ value.

The formulas that connect all relevant scalar masses to m_0 are collected in the Appendix, where more details about approximations and strategies for evaluating the sfermion spectrum can also be found. Since we are particularly interested in studying regions of the parameter space in which no pair-production processes of SUSY particles are allowed other than neutralino production, we choose to perform most of our analysis in scenarios with $m_0 \geq M_Z$. This choice has two important consequences. Firstly, for M_2 not too small (e.g., M_2 values not excluded by LEP 1 data), it gives rise to scalar masses greater than the LEP 2 beam energy, i.e., scalars cannot be pair produced at LEP 2 (cf. the Appendix). Secondly, with these relatively heavy scalars, the two-body decays $\tilde{\chi}_2^0 \to f\tilde{f}_{L,R}$ are in most cases not allowed. This point will be resumed in Secs. IV and V.

A general feature of $\tilde{\chi}_1^0\tilde{\chi}_2^0$ cross sections is that, in order to have a large contribution either from the s channel or the t channel (cf. Fig. 1), both $\tilde{\chi}_1^0$ and $\tilde{\chi}_2^0$ should have a large component of either Higgsinos or gauginos. Nevertheless, the t-channel contribution will be, in general, lower, especially when the selectron masses in the t-channel propagators are assumed larger than M_Z. Mixed cases, where the two neutralinos have different dominant components, give rise in general to comparable contribution from s, t amplitudes and their relative interference. The limit of production of one pure Higgsino plus one pure gaugino is dynamically forbidden and has a null cross section (for $m_e = 0$). These different cases will be discussed in what follows.

In Fig. 9, the contour plot of the total cross section (in fb) for $e^+e^- \to \tilde{\chi}_1^0\tilde{\chi}_2^0$ is shown for $\tan\beta = 1.5$, $m_0 = M_Z$ (which, for $M_2 = M_Z$, corresponds to $m_{\tilde{e}_L} = 124$ GeV and $m_{\tilde{e}_R} = 104$ GeV, cf. Table I), and $\sqrt{s} = 190$ GeV. We can distinguish different regions in the (μ, M_2) plane on the basis of the magnitude of the total cross section. The largest rates (up to about 2 pb) are reached for $|\mu| \lesssim M_Z$ and $M_2 \gtrsim M_Z$, where the two lightest neutralinos are mainly Higgsinos (with masses close to $\pm|\mu|$) and, hence, are fully coupled to the Z^0 in the s channel. In what follows, we will name the two regions in this area, on the left and on the right of the LEP

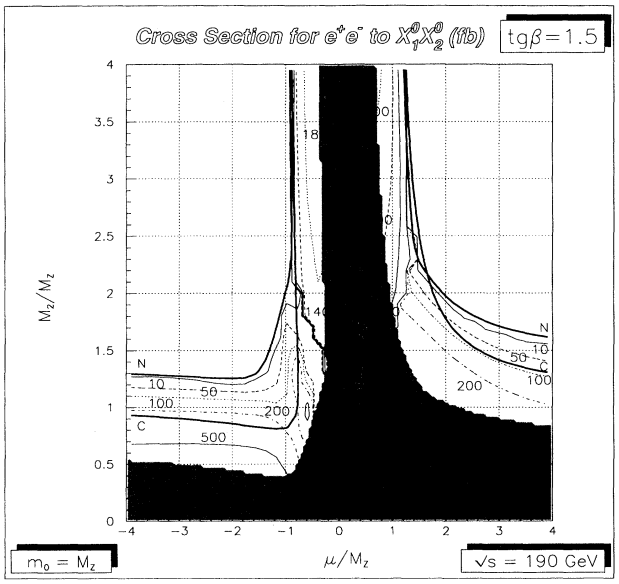

FIG. 9. Contour plot for the total cross section (in fb) of the process $e^+e^- \to \tilde{\chi}_1^0\tilde{\chi}_2^0$ at LEP 2 ($\sqrt{s} = 190$ GeV) on the (μ, M_2) plane in the $\tan\beta = 1.5$ $m_0 = M_Z$ case. The shaded area represents the region excluded by LEP 1 data.

1 excluded region, HCS$^-$ and HCS$^+$ (standing for high cross section) regions, respectively. These regions are shown in Fig. 7, where the contour plot for $\sigma(e^+e^- \to \tilde{\chi}_1^0\tilde{\chi}_2^0) = 1$ pb is also plotted, for $m_0 = M_Z$.

In the regions NR$^+$ and NR$^-$, the gaugino components and the related t-channel contribution to the total cross section come into play, and cross sections drop. Typical total rates in the regions NR$^-$ are of the order of 50–100 fb, corresponding to a number of about 25–50 events, for an integrated luminosity of 500 pb^{-1}. Somewhat lower cross sections are observed in the NR$^+$ region, where, because of the higher value of M_2, heavier selectrons are exchanged in the t channel [cf. Eqs. (A1), (A2), and Table I].

In Fig. 10, we show the effect of rising m_0 up to $3M_Z$. With respect to Fig. 9, cross sections are considerably reduced in regions where t-channel amplitudes are relevant. For instance, in the neutralino regions $\sigma(e^+e^- \to \tilde{\chi}_1^0\tilde{\chi}_2^0)$ is at most of the order of 20–30 fb. A moderate change is observed when varying the value of $\tan\beta$ up to 4 (Fig. 11), due mainly to the different NR$^+$ and NR$^-$ position and shape in the (μ, M_2) plane.

In order to clarify the origin of the total cross-section behavior in the (μ, M_2) plane and, in particular, in the NR$^\pm$ and high cross-section (HCS$^\pm$) regions, we consider now in detail a set of specific cases in the parameter space. In Table I, we report the following features for six different scenarios (A,B,C,D in the neutralino regions and $H^\pm$ in the HCS regions), defined by their values of μ and M_2 for $\tan\beta = 1.5$: (i) values of neutralino and chargino masses (including the correct sign), (ii) the percentage components of different gaugino and Higgsino physical states for $\tilde{\chi}_1^0$ and $\tilde{\chi}_2^0$, (iii) scalar masses arising from $m_0 = M_Z$ and RGE

evolution, calculated by Eqs. (A1) and (A2), (iv) total cross sections (in fb), for $m_0 = M_Z$ and $\sqrt{s} = 190$ GeV, of all the allowed neutralino-pair production processes, $e^+e^- \to \tilde{\chi}_1^0\tilde{\chi}_1^0$, $\tilde{\chi}_1^0\tilde{\chi}_2^0$ and, when below threshold, $\tilde{\chi}_1^0\tilde{\chi}_3^0$, $\tilde{\chi}_1^0\tilde{\chi}_4^0$, $\tilde{\chi}_2^0\tilde{\chi}_2^0$, and (v) for the main $\tilde{\chi}_1^0\tilde{\chi}_2^0$ channel, different contributions to the total rates coming from s channel, $(t+u)$ channels, and $(st+su)$ interferences. The location of the six points in the (μ, M_2) plane is shown in Fig. 7.

We now analyze the physical features of these scenarios. In scenario A, where $\mu = -3M_Z$ and $M_2 = M_Z$, the lightest neutralino is mostly a gaugino with a predominance of photinos. The next-to-lightest neutralino is still a gaugino, but with inverse $\tilde{\gamma}$-$\tilde{Z}$ relative composition. In this case, since $|\mu| \gg M_2, M_Z$, masses obey the asymptotic relation $m_{\tilde{\chi}_1^\pm} \simeq m_{\tilde{\chi}_2^0} \simeq 2m_{\tilde{\chi}_1^0}$. In such a scenario, the $\tilde{\chi}_1^0\tilde{\chi}_2^0$ cross section comes uniquely from t and u channels and is about 146 fb. In scenario B, where $\mu = -M_Z$ and $M_2 = M_Z$, there is a mixed sit-

TABLE I. Interesting scenarios for neutralino production at LEP 2 ($\sqrt{s} = 190$ GeV) in the $\tan\beta = 1.5$, $m_0 = M_Z$ case. Mass eigenvalues for charginos and neutralinos are given as well as sfermion spectrum arising from $m_0 = M_Z$. For light neutralinos, the physical composition and the total cross section (in fb) are also reported for all allowed pair-production processes $e^+e^- \to \tilde{\chi}_i^0\tilde{\chi}_j^0$. For the $\tilde{\chi}_1^0\tilde{\chi}_2^0$ case, individual contributions from s, $(t+u)$ channels and $(st+su)$ interferences are also given.

		Scenarios with $\tan\beta = 1.5$					
Scenario		A	B	C	D	H^-	H^+
$(\mu, M_2)/M_Z \to$		$(-3, 1)$	$(-1, 1)$	$(-1, 1.5)$	$(3, 1.5)$	$(-0.7, 3)$	$(1, 3)$
M_1 (GeV) $\to$		45.7	45.7	68.6	68.6	137.2	137.2
$\tilde{\chi}_1^0$	Mass (GeV)	49.5	51.5	73.7	56.0	62.3	44.9
	$(\tilde{\gamma}, \tilde{Z})$ (%)	(88, 11)	(91, 6)	(76, 10)	(47, 45)	(0, 1)	(4, 20)
	$(\tilde{H}_a^0, \tilde{H}_b^0)$ (%)	(1, 0)	(2, 2)	(1, 13)	(7, 1)	(2, 97)	(70, 5)
$\tilde{\chi}_2^0$	Mass (GeV)	107.0	85.2	89.8	108.2	−89.1	−92.3
	$(\tilde{\gamma}, \tilde{Z})$ (%)	(12, 83)	(4, 9)	(15, 1)	(53, 36)	(0, 7)	(0, 0)
	$(\tilde{H}_a^0, \tilde{H}_b^0)$ (%)	(4, 2)	(0, 86)	(2, 83)	(10, 1)	(90, 2)	(5, 94)
$\tilde{\chi}_3^0$	Mass (GeV)	275.4	−129.8	−124.5	−274.4	144.9	153.5
$\tilde{\chi}_4^0$	Mass (GeV)	−294.9	130.0	166.4	315.6	292.6	304.6
$\tilde{\chi}_1^\pm$	Mass (GeV)	106.1	104.7	110.8	−101.5	80.1	−62.6
$\tilde{\chi}_2^\pm$	Mass (GeV)	291.2	136.2	166.2	310.0	292.2	303.5
$\tilde{e}_L, \tilde{e}_R, \tilde{\nu}_{e,L}$	Mass (GeV)	124, 104, 114		152, 115, 144		255, 160, 250	
$\tilde{u}_L, \tilde{u}_R$	Mass (GeV)	285, 277		408, 395		773, 746	
$\tilde{d}_L, \tilde{d}_R$	Mass (GeV)	289, 278		411, 395		774, 743	
$\sigma(\tilde{\chi}_1^0\tilde{\chi}_1^0)$	Total (fb)	881.7	770.9	213.2	448.3	6.6	6.7
$\sigma(\tilde{\chi}_1^0\tilde{\chi}_2^0)$	Total	146.4	112.8	80.9	56.1	1654	1400
	(s) channel(fb)	0.1	18.1	9.1	0.1	1622	1366
	$(t+u)$ channels	142.7	48.1	38.9	51.8	0.3	0.4
	Interferences	3.6	46.5	32.8	4.2	31.0	33.4
$\sigma(\tilde{\chi}_1^0\tilde{\chi}_3^0)$	Total (fb)		176.7				
$\sigma(\tilde{\chi}_1^0\tilde{\chi}_4^0)$	Total (fb)		22.3				
$\sigma(\tilde{\chi}_2^0\tilde{\chi}_2^0)$	Total (fb)		4.8	0.4		0.3	0.1

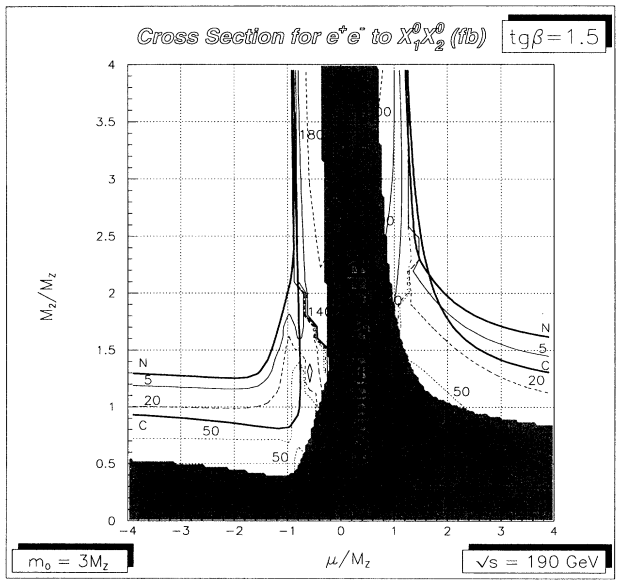

FIG. 10. Contour plot for the total cross section (in fb) of the process $e^+e^- \to \tilde{\chi}_1^0\tilde{\chi}_2^0$ at LEP 2 ($\sqrt{s} = 190$ GeV) on the (μ, M_2) plane in the $\tan\beta = 1.5$, $m_0 = 3M_Z$ case.

uation, where $\tilde{\chi}_1^0$ is predominantly a photino, while $\tilde{\chi}_2^0$ is mostly an $\tilde{H}_b^0$. The total $\tilde{\chi}_1^0\tilde{\chi}_2^0$ production rate receives contributions from all channels and interferences and is about 113 fb. One can notice that in this case the production cross section for $\tilde{\chi}_1^0\tilde{\chi}_3^0$ pairs is larger than for $\tilde{\chi}_1^0\tilde{\chi}_2^0$, although $m_{\tilde{\chi}_3^0}$ is much heavier than $m_{\tilde{\chi}_2^0}$. This is due to the different composition of $\tilde{\chi}_3^0$, i.e., its sizable gaugino component, which enhances the couplings to $\tilde{e}_{L,R}$ in the t channel. Scenario C is similar to B, but

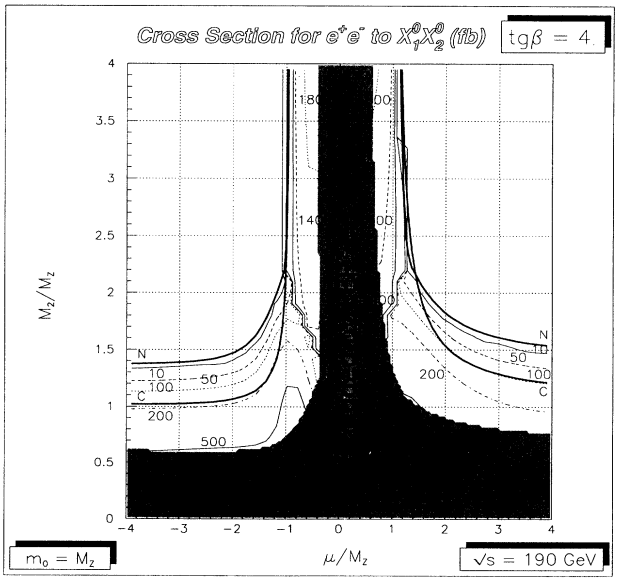

FIG. 11. Contour plot for the total cross section (in fb) of the process $e^+e^- \to \tilde{\chi}_1^0\tilde{\chi}_2^0$ at LEP 2 ($\sqrt{s} = 190$ GeV) on the (μ, M_2) plane in the $\tan\beta = 4$, $m_0 = M_Z$ case.

with a larger M_2 ($M_2 = 1.5M_Z$), which gives a heavier $\tilde{\chi}_1^0$ and consequently a smaller cross section. The scenario D ($\mu = 3M_Z$, $M_2 = 1.5M_Z$) is almost symmetrical to A under the transformation $\mu \to -\mu$ and gives both $\tilde{\chi}_1^0$ and $\tilde{\chi}_2^0$, made mostly of gauginos (with no really predominant $\tilde{\gamma}$ or $\tilde{Z}$ component) and lower production rates. Scenarios $H^\pm$ are both in the HCS regions. Here both $\tilde{\chi}_1^0$ and $\tilde{\chi}_2^0$ are predominantly Higgsinos (of different kinds), and we get quite large cross sections ($\sigma \approx 1.5$ pb). On the other hand, the rates for $\tilde{\chi}_1^0\tilde{\chi}_1^0$ production are quite small, since for $\tan\beta$ not far from 1 one needs different Higgsino components in the two produced neutralinos in order to get a large coupling to Z^0.

A similar analysis has been carried out in Table II, for $\tan\beta = 4$. The corresponding six different scenarios E, F, G, J in NR and $H^\pm$ in HCS are shown in Fig. 8.

We have also studied the m_0 and $\sqrt{s}$ dependence of $e^+e^- \to \tilde{\chi}_1^0\tilde{\chi}_2^0$ cross sections for the six scenarios with $\tan\beta = 1.5$. In Fig. 12, for $\sqrt{s} = 190$ GeV, we show the variation of cross sections with m_0. One can see that Scenarios A, B, C, and D, where the t channel amplitude is important, are the most affected by the m_0 value. The maximal sensitivity is found in case A, where the gaugino components are dominant in both $\tilde{\chi}_1^0$ and $\tilde{\chi}_2^0$. On the other hand, production rates for scenarios $H^\pm$ are quite insensitive to m_0, because of the s-channel dominance.

In Fig. 13, for $m_0 = M_Z$, the $\sqrt{s}$ dependence is studied around LEP 2 energies. Here too, one can notice the different behavior in various scenarios because of the relative importance of t- and s-channel contributions. For each curve, the magnified symbols denote situations in which the corresponding scenario is inside the neutralino regions (i.e., neutralino production is allowed, but chargino production is not).

IV. NEXT-TO-LIGHTEST NEUTRALINO DECAYS

In order to study possible signatures for $\tilde{\chi}_1^0\tilde{\chi}_2^0$ production at LEP 2, one has to analyze different decay channels for the next-to-lightest neutralino. Indeed, while $\tilde{\chi}_1^0$ will always produce a considerable missing energy and missing momentum signal, $\tilde{\chi}_2^0$ can give rise to a rich spectrum of final states [16,17]. In Ref. [7], a thorough study of all possible $\tilde{\chi}_2^0$-decay channels that are relevant at LEP 2 has been performed. The results of this analysis will be used in Sec. V for the evaluation of total rates for different final states corresponding to $\tilde{\chi}_1^0\tilde{\chi}_2^0$ production at LEP 2. On the other hand, in this section, we report explicit results for $\tilde{\chi}_2^0$ branching ratios (BR's), restricting ourselves to the particular scenarios introduced in Sec. III.

In the first column of Table III, all $\tilde{\chi}_2^0$ decays allowed in the MSSM are listed. The first two channels refer to the possibility for the $\tilde{\chi}_2^0$ to decay into either the lightest Higgs scalar h^0 or the Higgs pseudoscalar A^0 [18]. For this reason, in Table III, we choose different values for m_{A^0}, which fix, with $\tan\beta$, the spectrum and couplings of the Higgs sector. The following three channels include the main three-body processes, which occur through the

exchange of either a Z^0 gauge boson or a scalar particle [19]. These latter decays may occur in two steps, through production of a real scalar and its subsequent decay into the corresponding fermion and a $\tilde{\chi}_1^0$. In fact, although we are assuming $m_0 \geq M_Z$ so that $m_{\tilde{f}} > \sqrt{s}/2$, when m_0 is close to M_Z, one or more sleptons (usually the right selectron and sometimes the sneutrinos that are the lightest sfermions, cf. the Appendix) may turn out to be lighter than the $\tilde{\chi}_2^0$. We do not consider these situations separately and simply add these "on-shell" two-body contributions to the "off-shell" three-body ones. Of course, the on-shell two-body decay considerably enhances the corresponding BR. In the following two lines, we also show BR's of $\tilde{\chi}_2^0$ decays into a light chargino plus either leptons or hadrons, when allowed by phase space. The last channel is the one-loop radiative $\tilde{\chi}_2^0$ decay into a photon plus a $\tilde{\chi}_1^0$ [17], that gives rise in the $\tilde{\chi}_1^0\tilde{\chi}_2^0$ process to the nice signature of one single photon production. This channel at LEP 2 turns out to be, in general, potentially less important than at LEP 1. Further details on $B(\tilde{\chi}_2^0 \to \tilde{\chi}_1^0\gamma)$ can be found in Ref. [7].

Let's start by considering situations where Higgs bosons do not contribute to two-body $\tilde{\chi}_2^0$ decays and the dominant channels are $\tilde{\chi}_2^0 \to \ell^+\ell^-\tilde{\chi}_1^0$, $\nu_\ell\bar{\nu}_\ell\tilde{\chi}_1^0$, $q\bar{q}\tilde{\chi}_1^0$ in the neutralino region scenarios. In our framework, given $\tan\beta$ (that is equal to 1.5 in Table III) and M_2, all sfermion masses are fixed by the value of m_0. As a consequence, at fixed m_0, squark masses are much heavier than slepton masses, and the $\tilde{\chi}_2^0$ decay into hadrons coming from sfermion exchange are depressed with respect to

TABLE II. Interesting scenarios for neutralino production at LEP 2 ($\sqrt{s}$ = 190 GeV) in the $\tan\beta = 4$, $m_0 = M_Z$ case. See Table I for explanations.

		Scenarios with $\tan\beta = 4$					
Scenario		E	F	G	J	H^-	H^+
$(\mu, M_2)/M_Z \to$		$(-3, 1.1)$	$(-1.5, 1.5)$	$(2, 1.7)$	$(3, 1.3)$	$(-0.7, 3)$	$(1, 3)$
M_1 (GeV) $\to$		50.3	68.6	77.7	59.4	137.2	137.2
$\tilde{\chi}_1^0$	Mass (GeV)	52.1	68.1	62.7	53.0	53.5	55.7
	$(\tilde{\gamma}, \tilde{Z})$ (%)	(81, 17)	(66, 21)	(40, 41)	(57, 37)	(1, 5)	(4, 16)
	$(\tilde{H}_a^0, \tilde{H}_b^0)$ (%)	(0, 2)	(0, 13)	(9, 10)	(2, 3)	(14, 80)	(48, 32)
$\tilde{\chi}_2^0$	Mass (GeV)	102.9	107.3	113.8	99.4	−84.3	−98.6
	$(\tilde{\gamma}, \tilde{Z})$ (%)	(19, 72)	(30, 19)	(58, 18)	(43, 47)	(0, 6)	(0, 2)
	$(\tilde{H}_a^0, \tilde{H}_b^0)$ (%)	(0, 8)	(6, 45)	(15, 9)	(5, 5)	(75, 18)	(32, 66)
$\tilde{\chi}_3^0$	Mass (GeV)	285.5	−159.5	−189.6	−279.5	146.8	152.1
$\tilde{\chi}_4^0$	Mass (GeV)	−289.9	189.4	245.8	305.1	294.8	301.6
$\tilde{\chi}_1^\pm$	Mass (GeV)	103.2	111.8	−103.5	−96.7	69.5	−72.8
$\tilde{\chi}_2^\pm$	Mass (GeV)	295.2	194.4	243.8	304.0	294.9	301.2
$\tilde{e}_L$	Mass (GeV)	134	156	168	144	257	
$\tilde{e}_R$	Mass (GeV)	111	119	124	115	163	
$\tilde{\nu}_{e,L}$	Mass (GeV)	111	137	151	124	246	
$\tilde{u}_L$	Mass (GeV)	307	406	455	357	772	
$\tilde{u}_R$	Mass (GeV)	300	395	442	347	745	
$\tilde{d}_L$	Mass (GeV)	316	413	461	364	775	
$\tilde{d}_R$	Mass (GeV)	301	395	442	348	743	
$\sigma(\tilde{\chi}_1^0\tilde{\chi}_1^0)$	Total (fb)	731.7	268.3	215.9	545.3	42.7	19.8
$\sigma(\tilde{\chi}_1^0\tilde{\chi}_2^0)$	Total	111.2	40.6	33.8	88.7	1688	1307
(fb)	(s) channel	0.7	3.7	0.9	1.0	1617	1236
	$(t+u)$ channels	99.3	20.9	25.4	71.6	1.6	2.1
	Interferences	11.1	16.1	7.5	16.1	69.7	69.1
$\sigma(\tilde{\chi}_2^0\tilde{\chi}_2^0)$	Total (fb)					3.3	

Z^0-exchange contributions. In scenarios A and D, where $|\mu|$ is relatively high and gaugino components of $\tilde{\chi}_1^0$ and $\tilde{\chi}_2^0$ are dominant (cf. Table I), only sfermion exchange plays a role, and leptonic channels almost saturate $\tilde{\chi}_2^0$ decays. Notice that the numbers relative to the $e^+e^-\tilde{\chi}_1^0$ channel refer to only one species of charged leptons, while neutrino and quark channels are summed up over all light flavors. Since the right selectron is lighter than $\tilde{\chi}_2^0$ in scenario A and not too much heavier than $\tilde{\chi}_2^0$ in scenario D (cf. Table I), the BR for $\tilde{\chi}_2^0 \to \tilde{\chi}_1^0 \ell^+ \ell^-$ decay turns out to be very large and of the order of 75%, when summed up over three charged lepton species. On the other hand, scenarios B and C present mixed features, and leptonic channels are altogether comparable to the hadronic one. Decays into chargino are not relevant in the above scenarios, while the radiative $\tilde{\chi}_2^0 \to \tilde{\chi}_1^0 \gamma$ decay reaches a few percent of BR only in the B and C cases, where the total $\tilde{\chi}_2^0$ width is small due to the mixed gaugino-Higgsino nature of $\tilde{\chi}_1^0$ and $\tilde{\chi}_2^0$. As for scenario H^-, where Higgsino components are dominant, the Z^0 exchange saturates $\tilde{\chi}_2^0$ decays. Hence, BR's for various channels closely reflect the branching ratios for $Z^0 \to f\bar{f}$. In scenario H^+, the Z^0-channel dominance is less pronounced. Also, there is a considerable BR for channels with a $\tilde{\chi}_1^\pm$ in the final state, which gives rise to $\tilde{\chi}_2^0$ cascade decays.

When Higgs boson masses are sufficiently light to allow the decays $\tilde{\chi}_2^0 \to \tilde{\chi}_1^0 h^0$, $\tilde{\chi}_1^0 A^0$, these channels are always important. For instance, in the case A with $m_{A^0} = M_Z$, there is a 98% probability for $\tilde{\chi}_2^0 \to \tilde{\chi}_1^0 h^0$ (see Table III). In the case H^+ with $m_{A^0} = M_Z/2$, the BR for $\tilde{\chi}_2^0 \to \tilde{\chi}_1^0 A^0$ is about 21%. In general, Higgs channels will give rise to an enhanced hadronic signal coming from $h^0, A^0 \to b\bar{b}$. For $\tilde{\chi}_2^0$ decays into Higgs bosons, the h^0 mass and couplings have been computed taking into account the leading one-loop corrections due to top-quark-top-squark contributions in the approximation of degenerate top squark masses (cf. the Appendix).

A rather different picture emerges for $\tan\beta = 4$ (Table IV). First of all, when moving up from $\tan\beta = 1$, it is harder and harder to find scenarios where one of the two lightest neutralinos is almost a pure gaugino and the other one is almost a pure Higgsino in the parameter space relevant for LEP 2. Consequently, the tree-level decays of $\tilde{\chi}_2^0$ are never much depressed, and the BR for

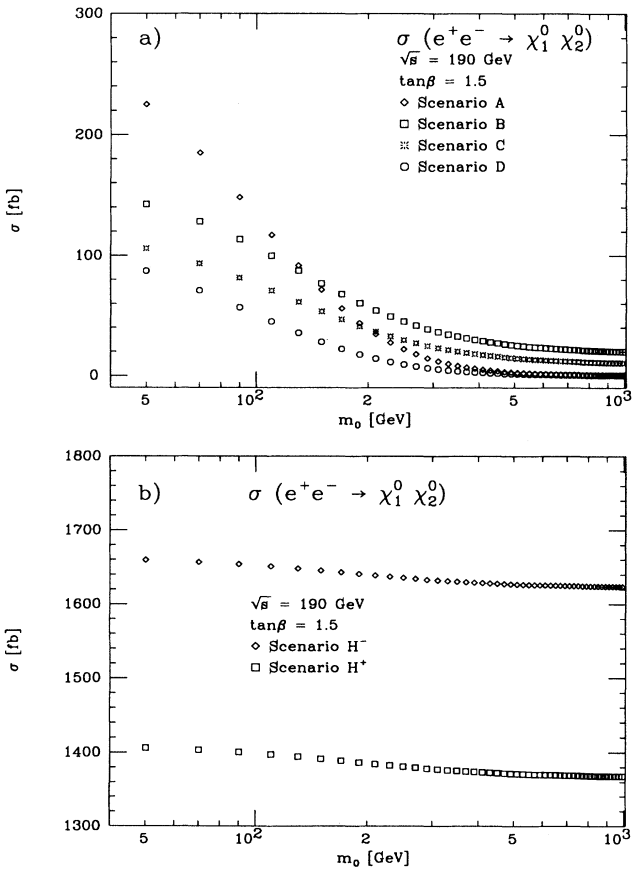

FIG. 12. Total cross section (in fb) of the process $e^+e^- \to \tilde{\chi}_1^0\tilde{\chi}_2^0$ as a function of m_0 (or, once M_2 is fixed, of the selectron masses) in the scenarios defined in Table I for $\tan\beta = 1.5$: (a) A, B, C, D and (b) H^-, H^+. Here the c.m. energy is $\sqrt{s} = 190$ GeV.

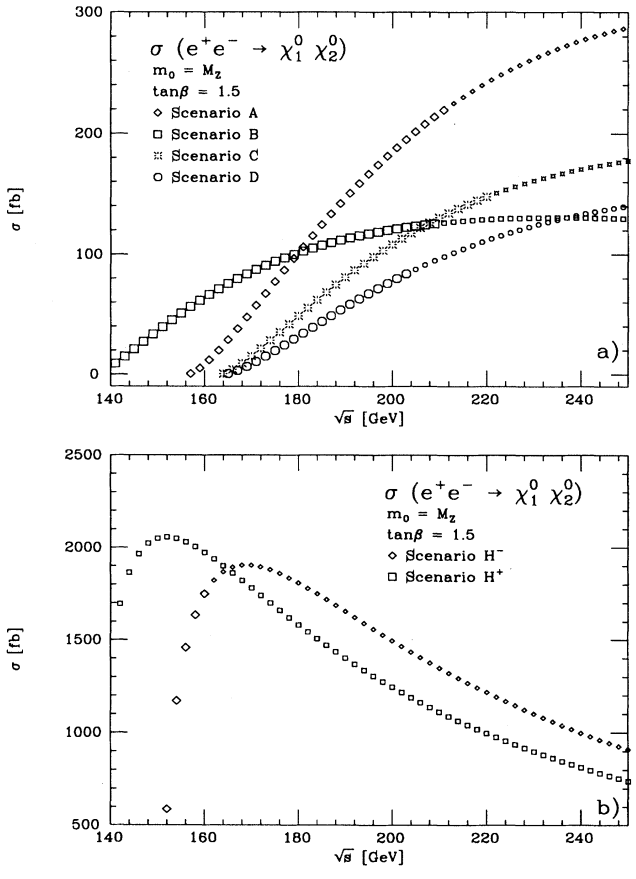

FIG. 13. Total cross section (in fb) of the process $e^+e^- \to \tilde{\chi}_1^0\tilde{\chi}_2^0$ as a function of $\sqrt{s}$ in the LEP 2 range in the scenarios defined in Table I, for $\tan\beta = 1.5$: (a) A, B, C, D and (b) H^-, H^+. The selectron masses are fixed by $m_0 = M_Z$. Large symbols are used when a scenario falls inside the $\mathrm{NR}^\pm$ regions.

TABLE III. Branching ratios (%) for $\tilde{\chi}_2^0$ decays in the scenarios with $\tan\beta = 1.5$, defined in Sec. III. Sfermion masses are fixed by $m_0 = M_Z$ and the indicated value of m_{A^0} sets the Higgs spectrum.

Branching ratios (%) for $\tilde{\chi}_2^0$ decays ($\tan\beta = 1.5$)										
Scenario	A		B		C		D	H^-	H^+	
$(\mu, M_2)/M_Z \rightarrow$	$(-3, 1)$		$(-1, 1)$		$(-1, 1.5)$		$(3, 1.5)$	$(-0.7, 3)$	$(1, 3)$	
m_{A^0} (GeV) $\rightarrow$	M_Z	$3M_Z$	M_Z	$3M_Z$	M_Z	$3M_Z$	$\gtrsim 75$	$\gtrsim 27$	$M_Z/2$	M_Z
$\tilde{\chi}_1^0 h^0$	97.6									
$\tilde{\chi}_1^0 A^0$									21.2	
$\tilde{\chi}_1^0 e^+ e^-$	0.6	26.6	2.8	2.7	9.9	9.7	25.9	3.3	2.0	2.5
$\sum_\ell \tilde{\chi}_1^0 \nu_\ell \bar{\nu}_\ell$	0.5	19.4	6.9	6.8	12.6	12.3	20.0	20.3	12.1	15.3
$\sum_{q \neq t} \tilde{\chi}_1^0 q\bar{q}$		0.5	80.9	79.8	51.7	50.6	1.7	67.7	40.2	51.0
$\tilde{\chi}_1^\pm e^\mp \bar{\nu}_e(\nu_e)$							0.1	0.2	2.3	2.9
$\sum_{(q,q') \neq t} \tilde{\chi}_1^\pm q\bar{q}'$							0.2	1.1	13.7	17.4
$\tilde{\chi}_1^0 \gamma$		0.2	3.8	5.1	6.0	7.9	0.1	0.5		
All visible	99.5	80.6	93.1	93.2	87.4	87.7	80.0	79.7	87.9	84.7

the radiative channel $\tilde{\chi}_2^0 \rightarrow \tilde{\chi}_1^0 \gamma$ can be at most a few per mil in the neutralino region. Furthermore, varying $\tan\beta$ changes both the gaugino-Higgsino composition of $\tilde{\chi}_{1,2}^0$ and the scalar mass spectrum. One of the main effects of that is the relative decreasing of the sneutrino mass with respect to selectron masses (cf. the Appendix).

In Table IV, one can see that in scenarios E and J with large $|\mu|$ and for heavy Higgs bosons, the BR for $\tilde{\chi}_2^0 \rightarrow \tilde{\chi}_1^0 \nu_\ell \bar{\nu}_\ell$ turns out to be considerably enhanced and decreases the visible fraction of $\tilde{\chi}_2^0$ decays. As for decays into real Higgs bosons, one should take into account that the h^0 mass increases with $\tan\beta$ at fixed m_{A^0} [cf. Eqs. (A6)]. For this reason, in Table IV, lower values of m_{A^0} with respect to Table III have been chosen to characterize scenarios with allowed and not-allowed $\tilde{\chi}_2^0 \rightarrow \tilde{\chi}_1^0 h^0$, $\tilde{\chi}_1^0 A^0$ decays. Here again, when permitted by phase space, the two-body decay into Higgs bosons almost saturates the BR.

As in the case $\tan\beta = 1.5$, the detailed features of each decay BR in Table IV can be understood by considering the physical composition of neutralinos given in Table II, for scenarios with $\tan\beta = 4$.

TABLE IV. The same as in Table III, but for $\tan\beta = 4$.

Branching ratios (%) for $\tilde{\chi}_2^0$ decays ($\tan\beta = 4$)										
Scenario	E		F	G		J		H^-	H^+	
$(\mu, M_2)/M_Z \rightarrow$	$(-3, 1.1)$		$(-1.5, 1.5)$	$(2, 1.7)$		$(3, 1.3)$		$(-0.7, 3)$	$(1, 3)$	
m_{A^0} (GeV) $\rightarrow$	$M_Z/2$	M_Z	Any	$M_Z/2$	M_Z	$M_Z/2$	M_Z	Any	$\gtrsim 43$	
$\tilde{\chi}_1^0 h^0$	97.9			98.6		99.8				
$\tilde{\chi}_1^0 A^0$	1.8			1.4		0.2				
$\tilde{\chi}_1^0 e^+ e^-$		8.8	11.1		25.6		12.3	3.0	2.6	
$\sum_\ell \tilde{\chi}_1^0 \nu_\ell \bar{\nu}_\ell$	0.2	70.1	0.6		1.4		55.6	18.9	16.1	
$\sum_{q \neq t} \tilde{\chi}_1^0 q\bar{q}$		3.4	65.6		19.1		7.4	62.6	53.1	
$\tilde{\chi}_1^\pm e^\mp \bar{\nu}_e(\nu_e)$					0.4			1.0	2.6	
$\sum_{(q,q') \neq t} \tilde{\chi}_1^\pm q\bar{q}'$					1.7			6.1	15.4	
$\tilde{\chi}_1^0 \gamma$		0.2	0.6					0.2		
All visible	99.8	29.9	99.4	100	98.6	100	44.4	81.1	83.9	

V. TOTAL RATES FOR DIFFERENT $\tilde{\chi}_1^0\tilde{\chi}_2^0$ SIGNATURES

In this section, we will show results on total rates corresponding to different signatures coming from the process $e^+e^- \to \tilde{\chi}_1^0\tilde{\chi}_2^0$, with particular emphasis on the neutralino regions. Various rates are obtained by multiplying cross sections with BR's for different decay channels of $\tilde{\chi}_2^0$ at fixed values of M_2, μ, m_0, $\tan\beta$, and m_{A^0}.

While $\tilde{\chi}_1^0$ always produces a large missing energy and missing momentum signal in the final state, each $\tilde{\chi}_2^0$ decay channel contributes to a different signature. The most interesting signatures correspond to some visible either leptonic or hadronic (less often mixed) signal concentrated in the opposite side with respect to the $\tilde{\chi}_1^0$ direction. In our analysis, we neglect hadronization effects, and, in general, we assume that each quark gives rise to a jet in the final state.

We now proceed to listing all the possible signatures corresponding to $e^+e^- \to \tilde{\chi}_1^0\tilde{\chi}_2^0$.

(i) $\ell^+\ell^-+ \not{E}$, coming, in general, from $\tilde{\chi}_2^0 \to \tilde{\chi}_1^0\ell^+\ell^-$ ($\ell = e, \mu$). The same signature, but with softer leptons, is obtained for particular scenarios where cascade decays of $\tilde{\chi}_2^0$ through a lighter $\tilde{\chi}_1^\pm$ are allowed:

$$\begin{array}{rcl} e^+e^- & \to & \tilde{\chi}_1^0\,\tilde{\chi}_2^0 \\ & & \quad\hookrightarrow \ell^\pm\nu_\ell\tilde{\chi}^\mp \\ & & \qquad\hookrightarrow \ell^\mp\nu_\ell\tilde{\chi}_1^0\,. \end{array} \tag{5.1}$$

We will see that these cascade decays are relevant in regions of the (μ, M_2) plane where also chargino-pair production can occur. By the way, the process (5.1) will give rise, with twice the BR for $\tilde{\chi}_2^0 \to \ell^+\ell^- + \tilde{\chi}_1^0$, to the signature $\ell^+\ell'^-+ \not{E}$ with a pair of leptons of different flavors. We also notice once more that our choice of m_0 (which prevents pair production of sleptons at LEP 2), hinders the two-body decay $\tilde{\chi}_2^0 \to \tilde{\ell}_{L,R}^\pm\ell^\mp$. Nevertheless, there are particular choices of SUSY parameters (e.g., scenario A) that allow the $\tilde{\chi}_2^0$ decay into a real charged slepton that is too heavy to be pair produced at LEP 2. The same can happen with the $\tilde{\chi}_2^0 \to \tilde{\nu}_{\ell,L}\bar{\nu}_\ell$, $\bar{\tilde{\nu}}_{\ell,L}\nu_\ell$ channel, but not for $\tilde{\chi}_2^0 \to \tilde{q}_{L,R}\bar{q}$, $\bar{\tilde{q}}_{L,R}q$, since squarks are generally much heavier than sleptons (cf. the Appendix). This is also supported by the stronger limits found by the Collider Detector at Fermilab (CDF) collaboration on $m_{\tilde{q}_{L,R}}$, with respect to the LEP limits on $m_{\tilde{\ell}_{L,R}}$ [20]. Correspondingly, one can have situations in which the leptonic decays almost saturate the $\tilde{\chi}_2^0$ width. In particular, if only $\tilde{\chi}_2^0 \to \bar{\tilde{\ell}}_R^\pm\ell^\mp$ is allowed, as in the scenario A ($\tilde{\ell}_R$ is, in general, lighter than $\tilde{\ell}_L$ and $\tilde{\nu}_{\ell,L}$), the $\ell^+\ell^-+ \not{E}$ signal is at least 25% of the total for each lepton flavor.

(ii) $2j+ \not{E}$, arising from the decay $\tilde{\chi}_2^0 \to q\bar{q}\tilde{\chi}_1^0$. Our results are always summed up over five quark flavors (in the massless-quark approximation). When allowed by phase space, also the two-body decays $\tilde{\chi}_2^0 \to \tilde{\chi}_1^0h^0$, $\tilde{\chi}_1^0A^0$ enter this class, because of the subsequent $h^0, A^0 \to b\bar{b}$. In our analysis, we will sum this contribution, when present, to the direct two-jet signal.

(iii) $\gamma+ \not{E}$, coming from the one-loop decay $\tilde{\chi}_2^0 \to \tilde{\chi}_1^0\gamma$.

(iv) $4j+ \not{E}$. This arises from the cascade decay $\tilde{\chi}_2^0 \to \tilde{\chi}_1^\pm(\to q_1\bar{q}_1'\tilde{\chi}_1^0)q_2\bar{q}_2'$, similarly to (5.1).

(v) $\ell^\pm + 2j+ \not{E}$, still coming from $\tilde{\chi}_2^0$ cascade decays $\tilde{\chi}_2^0 \to \tilde{\chi}_1^\mp(\to q\bar{q}'\tilde{\chi}_1^0)\ell^\pm\nu_\ell$ or $\tilde{\chi}_2^0 \to \tilde{\chi}_1^\pm(\to \ell^\pm\nu_\ell\tilde{\chi}_1^0)q\bar{q}'$.

(vi) invisible. This arises from channels that have only neutrinos and $\tilde{\chi}_1^0$'s in the final state, that is $\tilde{\chi}_2^0 \to \nu_\ell\bar{\nu}_\ell\tilde{\chi}_1^0$. Of course, this is the least interesting signature, which, at LEP 2, can be seen only if there is some detected radiation emitted from the initial state. This case is disfavored due to both a lower cross section corresponding to the initial state photon radiation and a smaller effective c.m. energy left for the $\tilde{\chi}_1^0\tilde{\chi}_2^0$ production. The latter effect takes the available parameter space back to the region covered by chargino search.

(vii) $\tau^+\tau^-+ \not{E}$. Most of the time, this signal arises from the direct decay $\tilde{\chi}_2^0 \to \tau^+\tau^-\tilde{\chi}_1^0$, analogously to the events of class (i) above. A non-negligible contribution to this channel comes also from direct decays $\tilde{\chi}_2^0 \to \tilde{\chi}_1^0h^0$, $\tilde{\chi}_1^0A^0$ when allowed by phase space. Tau production gives rise to various signatures, where, in general, the visible energy is lower than for previous cases because of the presence of at least two neutrinos in the final state. One can have a $\ell^+\ell^{(\prime)-}+ \not{E}$ signature, with a BR of about 12%, hadrons $+\not{E}$ with a 41% probability, and, in the remaining cases, $\ell^\pm+$ hadrons $+\not{E}$. In the following analysis, we will keep separate the contributions to hadronic and (e-μ) leptonic signals coming from τ decays from the main ones described in classes (i)–(v).

One should keep in mind that, in order to get a detectable signal arising from the above decay channels, the mass difference between $\tilde{\chi}_2^0$ and $\tilde{\chi}_1^0$ must be sizeable. Indeed, jets, leptons, and photons should have enough visible energy. We have checked that this condition is, in general, fulfilled in the region of the SUSY parameter space not excluded by LEP 1. A few exceptions occur in very limited regions for $\tan\beta \simeq 1$. This aspect can be more dramatic for jets and/or leptons arising from $\tilde{\chi}_2^0$ cascade decays through a light chargino. In this case, at least one of the two differences $(m_{\tilde{\chi}_2^0} - m_{\tilde{\chi}_1^\pm})$ and $(m_{\tilde{\chi}_1^\pm} - m_{\tilde{\chi}_1^0})$ should be sizeable. We will explicitly show unfavorable regions (which, in most cases, do not overlap with the parameter space explorable at LEP 2) in the following discussion.

In Figs. 14, 15, and 16, we show the contour plots in the (μ, M_2) plane for total rates (in fb) corresponding to signatures (i)–(iii), coming from direct (and, if relevant, from cascade) $\tilde{\chi}_2^0$ decays when $\tilde{\chi}_2^0$ two-body decays into Higgs bosons are not allowed. We set $\sqrt{s} = 190$ GeV, $m_0 = M_Z$, and $\tan\beta = 1.5$. The precise value of $m_{A^0} = 3M_Z$, besides pushing Higgs boson masses above threshold for $\tilde{\chi}_2^0 \to \tilde{\chi}_1^0h^0$, $\tilde{\chi}_1^0A^0$, is relevant for the single-photon signal, since charged Higgs bosons enter into loops for the radiative $\tilde{\chi}_2^0 \to \tilde{\chi}_1^0\gamma$ decay (larger $m_{H^\pm}$ gives higher rates for this signal, cf. Table III). With an integrated luminosity of 500 pb^{-1}, it is straightforward to get the expected number of events at LEP 2 by halving the numbers shown in the figures.

The thick bold line in Figs. 14, 15, and 16 binds the small area, where $(m_{\tilde{\chi}_2^0} - m_{\tilde{\chi}_1^0}) < 10$ GeV. This may help in selecting regions where the final particles are actually visible in all direct decays.

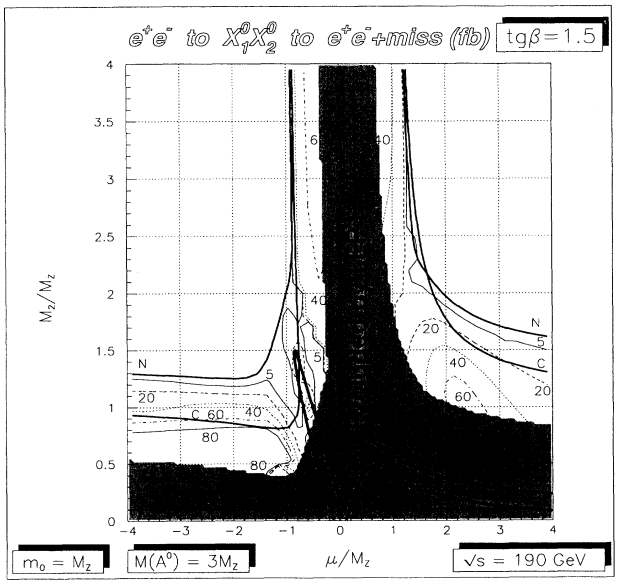

FIG. 14. Contour plot for the rate (in fb) of $e^+e^- \to \tilde{\chi}_1^0\tilde{\chi}_2^0 \to e^+e^- + \not{E}$ events at LEP 2 ($\sqrt{s} = 190$ GeV), in the case $\tan\beta = 1.5$, $m_0 = m_{A^0}/3 = M_Z$. Bold curves show kinematical limits for production of $\tilde{\chi}_1^+\tilde{\chi}_1^-$ (label "C") and of $\tilde{\chi}_1^0\tilde{\chi}_2^0$ (label "N"). The shaded area represents the region excluded by LEP 1 data. The thick bold line binds the region where $(m_{\tilde{\chi}_2^0} - m_{\tilde{\chi}_1^0}) < 10$ GeV.

As for the $e^+e^- + \not{E}$ signal, we can note in Fig. 14 that in the NR$^+$ one gets up to 60 fb (equivalent to 30 events), mainly because of the presence of a light selectron, while in the NR$^+$, rates reach at most 20 fb. Comparable rates are obtained in the high cross section regions HCS$^\pm$ because of the dominance of Z^0 channels, which keep the relevant leptonic $\tilde{\chi}_2^0$-decay BR's down to values of the order of $B(Z^0 \to e^+e^-)$.

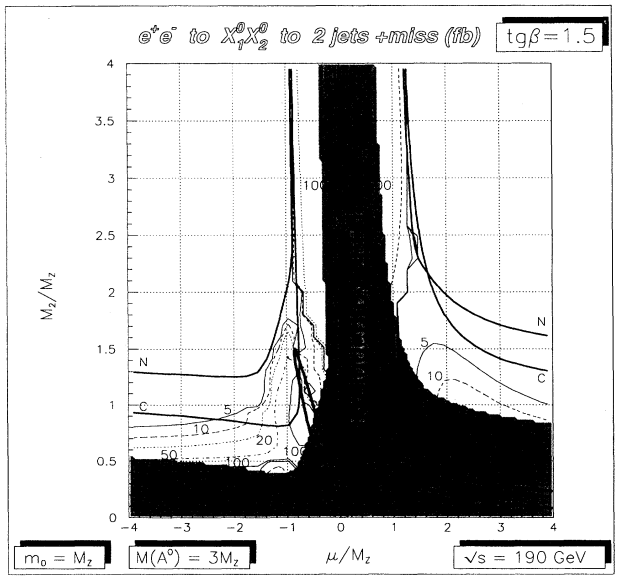

FIG. 15. Contour plot for the rate (in fb) of $e^+e^- \to \tilde{\chi}_1^0\tilde{\chi}_2^0 \to$ 2 jets $+\not{E}$ events. Notations and parameter values are the same as for Fig. 14.

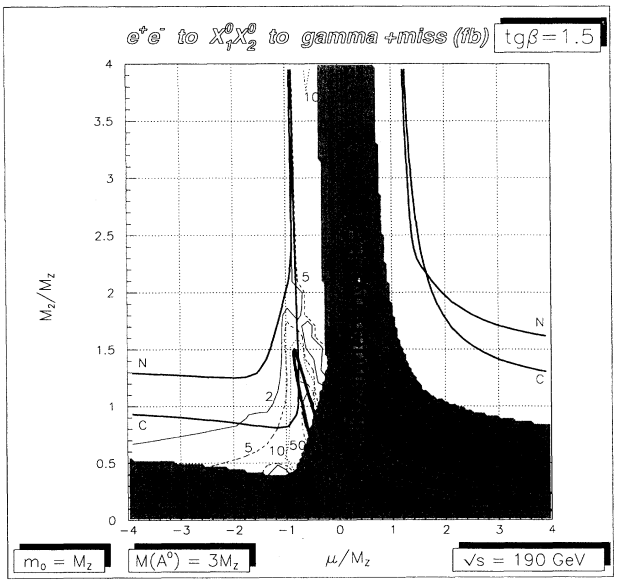

FIG. 16. Contour plot for the rate (in fb) of $e^+e^- \to \tilde{\chi}_1^0\tilde{\chi}_2^0 \to \gamma + \not{E}$ events. Notations and parameter values are the same as for Fig. 14.

A much less favorable situation is found for the 2j + $\not{E}$ signature for the same set of parameters. In Fig. 15, we can see that in most of the neutralino regions the rate for this signal is too low to be detected at LEP 2. In particular for $|\mu| > 2M_Z$ in the NR's, one finds less than 5 fb, while some signal can be detected in the NR$^+$ for $-2M_Z < \mu \lesssim M_Z$. In this region, where Z^0-channel $\tilde{\chi}_2^0$ decays (which are not depressed by squark masses) are important because of the quite large Higgsino component of $\tilde{\chi}_2^0$ (cf. Table I) rates up to 100 fb can be reached. Differently from the leptonic signature of Fig. 14, in the HCS regions the large value of $B(Z^0 \to q\bar{q})$ gives rise to total rates of the order of 1 pb.

In Fig. 16, the single photon rate coming from $\tilde{\chi}_2^0 \to \tilde{\chi}_1^0\gamma$ is shown. No signal is obtained for $\mu > 0$, while in the $\mu < 0$ half-plane one can reach at most about 100 fb in the region covered by the chargino search. Restricting ourselves to the NR$^+$, rates up to about 50 fb are found in the area close to $2\mu = -M_Z$, just on the edge of the chargino-pair-production region. Unfortunately, in the regions where the rate for the $\gamma + \not{E}$ signal exceeds 50 fb, the emitted photon is likely to be quite soft, due to the small difference between neutralino masses ($\lesssim 10$ GeV, see the thick bold line in Fig. 16). In the HCS regions, some signal is found only for $\mu < 0$ and very large M_2 values.

The total rate coming from all visible $\tilde{\chi}_2^0$-decay channels (including cascade decays, see below) is reported in Fig. 17, where the same set of SUSY parameters as for Figs. 14–16 has been chosen. By comparing this figure with Fig. 9 for total cross section, one can also assess rates from invisible $\tilde{\chi}_2^0$ decays, which for $\tan\beta = 1.5$ are typically 10–20 % of the total.

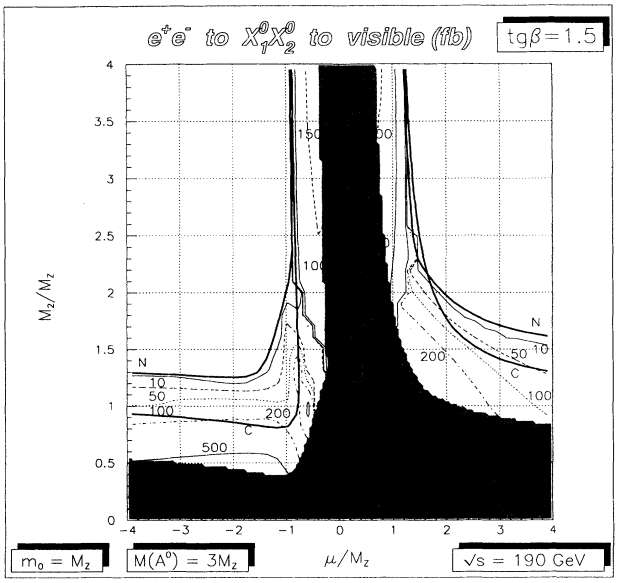

FIG. 17. Contour plot for the total rate (in fb) of visible events coming from $\tilde{\chi}_1^0\tilde{\chi}_2^0$ production at LEP 2. Notations and parameter values are the same as for Fig. 14.

The effect on the hadronic signal of assuming a lighter Higgs spectrum and, in particular, of allowing the decay $\tilde{\chi}_2^0 \to h^0\tilde{\chi}_1^0$ is shown in Fig. 18, which gives the $2j + \not{E}$ rates for $m_{A^0} = M_Z$ (the values of remaining parameters are the same as for Fig. 15). By comparing Figs. 18 and 15, one finds a remarkable enhancement of the hadronic signal in the (μ, M_2) parameter space, where the $\tilde{\chi}_2^0$-$\tilde{\chi}_1^0$ mass difference is larger than m_{h^0}. This mainly happens for $\mu < -M_Z$ in the neutralino regions. Hence, the bulk of the leptonic signal in the NR^+ is substituted by the two-jet signal (where the two jets are predominantly b-quark jets coming from $h^0 \to b\bar{b}$).

The rate for $4j + \not{E}$ arising from the cascade decay $\tilde{\chi}_2^0 \to \tilde{\chi}_1^{\pm}(\to q_1\bar{q}_1'\tilde{\chi}_1^0)q_2\bar{q}_2'$ is shown in Fig. 19, for $m_0 = M_Z$ and $\tan\beta = 1.5$. The heavy Higgs case is considered ($m_{A^0} = 3M_Z$). One can see that a considerable signal is found for positive μ, but not in regions not covered by direct chargino search. In the area not excluded by LEP 1, one gets rates up to about 200 fb.

In Fig. 19, outside the bold dashed line, one has $(m_{\tilde{\chi}_2^0} - m_{\tilde{\chi}_1^{\pm}}) < 10$ GeV, while the region where $(m_{\tilde{\chi}_1^{\pm}} - m_{\tilde{\chi}_1^0}) < 10$ GeV is completely contained in the area excluded by LEP 1. Therefore, one can hope to have a visible four-jet signal in most of the large-rate region, while at least two jets should be always detectable. An analogous conclusion applies to the other cascade-decay signatures.

The mixed semileptonic signature $e^+ + 2j + \not{E}$, still coming from $\tilde{\chi}_2^0$ cascade decays mediated by a light chargino, is studied in Fig. 20, for the same set of m_0, m_{A^0} and $\tan\beta$ values. Rates refer to a positron in the final state and must be doubled when summing up over lepton charges. The picture in the (μ, M_2) plane is similar to the previous $4j + \not{E}$ one, with lower rates mainly due to the single leptonic flavor considered. A similar behavior is also found for the $e^+\mu^- + \not{E}$ rates, which are, however, further reduced and at the edge of detectability.

Up to now, we considered the case $\tan\beta = 1.5$. Increasing the $\tan\beta$ value, in general, makes the situation worse because of the combined effects of the shift of the NR area (that for the larger $\tan\beta$ value tends to be more symmetric with respect to the inversion of the μ sign) and of the reduction of $\tilde{\chi}_2^0$ BR's for visible decays. In Fig. 21, the rates for the total visible signal are shown

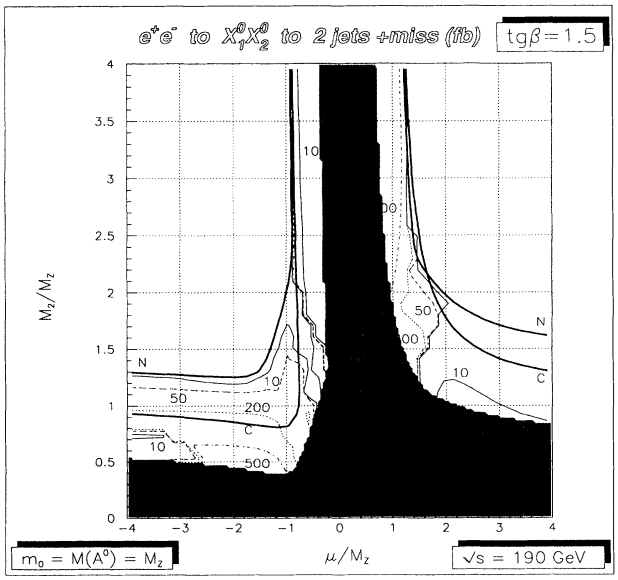

FIG. 18. Contour plot for the rate (in fb) of $e^+e^- \to \tilde{\chi}_1^0\tilde{\chi}_2^0 \to 2$ jets $+\not{E}$ events at LEP 2 ($\sqrt{s} = 190$ GeV), in the case $\tan\beta = 1.5$ and $m_0 = m_{A^0} = M_Z$.

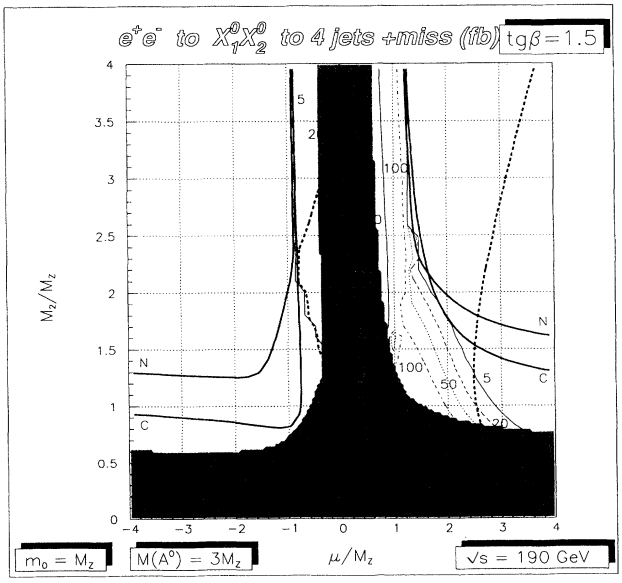

FIG. 19. Contour plot for the rate (in fb) of $e^+e^- \to \tilde{\chi}_1^0\tilde{\chi}_2^0 \to$ four jets $+\not{E}$ at LEP 2 ($\sqrt{s} = 190$ GeV), in the case $\tan\beta = 1.5$, $m_0 = M_Z$, and $m_{A^0} = 3M_Z$. Inside the bold dashed line, one has $(m_{\tilde{\chi}_2^0} - m_{\tilde{\chi}_1^{\pm}}) > 10$ GeV.

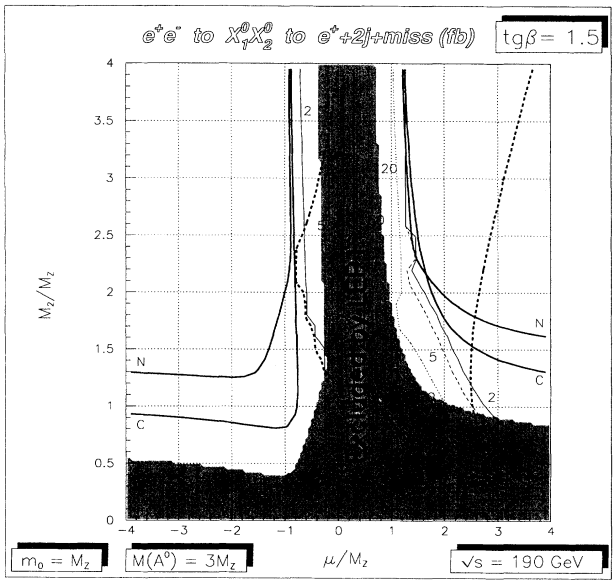

FIG. 20. Contour plot for the rate (in fb) of $e^+e^- \to \tilde{\chi}_1^0\tilde{\chi}_2^0 \to e^+ +$ two jets $+\not{E}$ events. Notations and parameter values are the same as for Fig. 19.

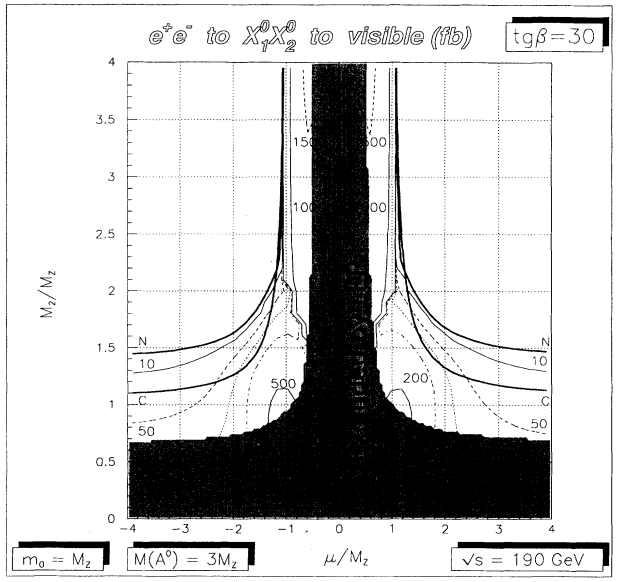

FIG. 22. Contour plot for the total rate (in fb) of visible events coming from $\tilde{\chi}_1^0\tilde{\chi}_2^0$ at LEP 2 ($\sqrt{s} = 190$ GeV), in the case $\tan\beta = 30$, $m_0 = M_Z$, and $m_{A^0} = 3M_Z$.

for $m_0 = M_Z$, $m_{A^0} = M_Z$, and $\tan\beta = 4$. The relatively light m_{A^0} in this case does not give rise to direct $\tilde{\chi}_2^0 \to \tilde{\chi}_1^0 h^0$ decays because of the strong dependence of m_{h^0} on $\tan\beta$ (cf. Table IV). One can see that the neutralino region rates are lower than for $\tan\beta = 1.5$ (cf. Fig. 17).

This trend is followed even for higher values of $\tan\beta$. For instance, in Fig. 22, the visible signal for $\tan\beta = 30$ and $m_0 = M_Z$, is shown. Here, the visible rate is greater than about 100 fb only outside the neutralino regions. The same pattern is observed for the $e^+e^- + \not{E}$ and two jets $+\not{E}$ rates. As for the $\gamma + \not{E}$ signal, its cross section never exceeds a few fb's outside the region covered by LEP 1, while rates for the four jets $+\not{E}$ cascade decay (which are similar to the $e^+ +$ 2 jets $+\not{E}$ ones) are shown in Fig. 23. As for the detectability of jets, leptons, and photons at high $\tan\beta$, we have checked that, for $\tan\beta \gtrsim 4$, neutralino- and chargino-mass differences

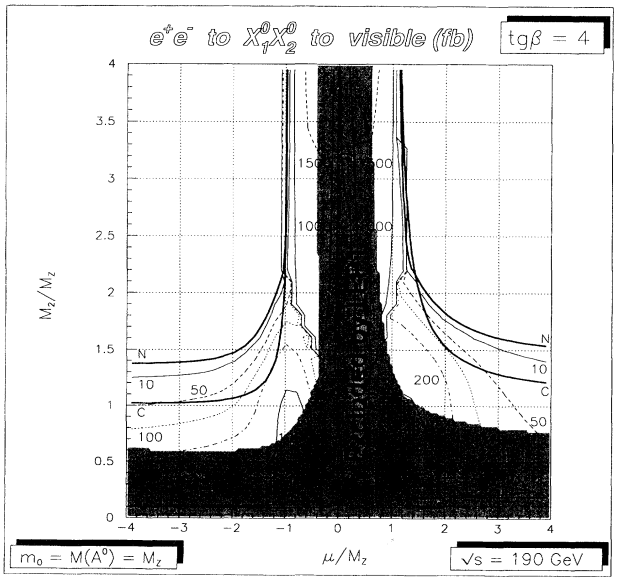

FIG. 21. Contour plot for the total rate (in fb) of visible events coming from $\tilde{\chi}_1^0\tilde{\chi}_2^0$ at LEP 2 ($\sqrt{s} = 190$ GeV), in the case $\tan\beta = 4$ and $m_0 = m_{A^0} = M_Z$.

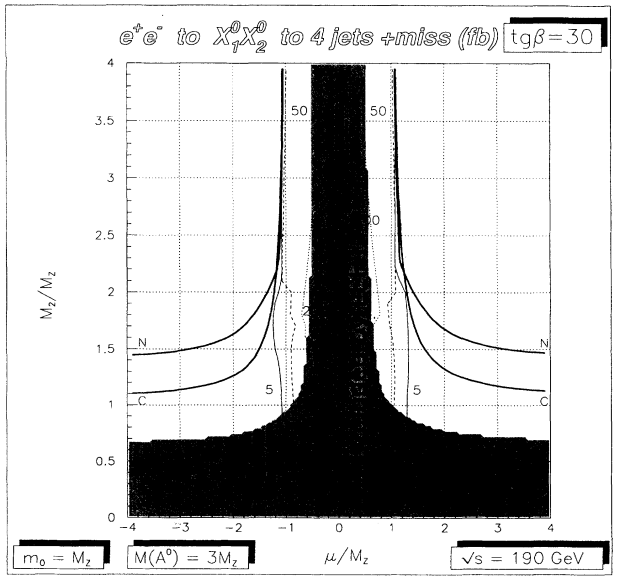

FIG. 23. Contour plot for the rate (in fb) of $e^+e^- \to \tilde{\chi}_1^0\tilde{\chi}_2^0 \to$ four jets $+\not{E}$ at LEP 2 ($\sqrt{s} = 190$ GeV), in the case $\tan\beta = 30$, $m_0 = M_Z$, and $m_{A^0} = 3M_Z$.

TABLE V. Total rates (in fb) corresponding to different signatures arising from $\tilde{\chi}_1^0\tilde{\chi}_2^0$ production at LEP 2 ($\sqrt{s}$ = 190 GeV) in the six significant scenarios with $\tan\beta = 1.5$ defined in Sec. III. Sfermion masses are fixed by $m_0 = M_Z$ and the indicated value of m_{A^0} sets the Higgs spectrum.

Rates (fb) for $e^+e^- \to \tilde{\chi}_1^0\tilde{\chi}_2^0 \to$ final state ($\tan\beta = 1.5$)										
Scenario	A		B		C		D	H^-	H^+	
$(\mu, M_2)/M_Z \to$	$(-3, 1)$		$(-1, 1)$		$(-1, 1.5)$		$(3, 1.5)$	$(-0.7, 3)$	$(1, 3)$	
m_{A^0} (GeV) $\to$	M_Z	$3M_Z$	M_Z	$3M_Z$	M_Z	$3M_Z$	$\gtrsim 75$	$\gtrsim 27$	$M_Z/2$	M_Z
$e^+e^- + \not{E}$	0.9	39.0	3.1	3.1	8.0	7.8	14.6	55.5	31.3	39.7
$e^+\mu^- + \not{E}$								0.3	3.6	4.6
Invisible	0.7	28.4	7.8	7.7	10.2	10.0	11.2	335.2	168.9	214.2
$\tau^+\tau^- + \not{E}$	6.9	39.0	3.1	3.1	8.0	7.8	14.6	55.5	31.9	39.7
$2j + \not{E}$	136.9	0.7	91.2	90.0	41.8	40.9	1.0	1120	858.9	714.2
$b\bar{b} + \not{E}$	133.5		18.5	18.2	8.9	8.7	0.3	246.0	419.3	156.9
$e^+ + 2j + \not{E}$								2.0	21.5	27.2
$4j + \not{E}$							0.1	11.6	127.5	161.7
$\gamma + \not{E}$		0.3	4.3	5.8	4.8	6.4		6.5		
All visible	145.7	118.0	104.9	105.0	70.7	70.9	44.9	1318	1231	1186

are always sufficient to provide enough energy to the final particles in regions relevant at LEP 2.

Finally, in Tables V and VI total rates corresponding to all possible signatures coming from $e^+e^- \to \tilde{\chi}_1^0\tilde{\chi}_2^0$ at LEP 2 are shown for the scenarios defined above with $\tan\beta = 1.5$ and $\tan\beta = 4$, respectively. Note that in these tables the rates relative to each signature include all possible contributions. For instance, $\tau^+\tau^- + \not{E}$ includes both the direct $\tilde{\chi}_2^0 \to \tau^+\tau^-\tilde{\chi}_1^0$ decay and the two processes $\tilde{\chi}_2^0 \to h^0, A^0(\to \tau^+\tau^-)\tilde{\chi}_1^0$ and $\tilde{\chi}_2^0 \to \tilde{\chi}_1^\pm(\to \tau^\pm\nu_\tau)\tau^\mp\nu_\tau\tilde{\chi}_1^0$.

We now make some comments on specific neutralino-region scenarios. In scenario A, for heavy Higgs bosons, one has a considerable leptonic signal, corresponding to about 40 $e^+e^-, \mu^+\mu^- + \not{E}$ events for 500 pb^{-1}. For light Higgs bosons, this is replaced by an even larger hadronic

TABLE VI. The same as in Table V, but for $\tan\beta = 4$.

Rates (fb) for $e^+e^- \to \tilde{\chi}_1^0\tilde{\chi}_2^0 \to$ final state ($\tan\beta = 4$)									
Scenario	E		F	G		J		H^-	H^+
$(\mu, M_2)/M_Z \to$	$(-3, 1.1)$		$(-1.5, 1.5)$	$(2, 1.7)$		$(3, 1.3)$		$(-0.7, 3)$	$(1, 3)$
m_{A^0} (GeV) $\to$	$M_Z/2$	M_Z	Any	$M_Z/2$	M_Z	$M_Z/2$	M_Z	Any	$\gtrsim 43$
$e^+e^- + \not{E}$		9.7	4.5		8.6		10.9	53.4	37.3
$e^+\mu^- + \not{E}$								1.9	3.8
Invisible	0.2	77.9	0.3		0.5		49.3	319.6	210.5
$\tau^+\tau^- + \not{E}$	4.8	9.7	4.5	1.4	8.6	3.9	10.9	53.4	37.3
$2j + \not{E}$	106.1	3.8	26.6	32.3	6.4	84.8	6.6	1057	693.4
$b\bar{b} + \not{E}$	105.9	0.7	5.8	32.2	1.5	84.6	1.6	232.0	152.2
$e^+ + 2j + \not{E}$					0.1			11.5	22.5
$4j + \not{E}$					0.3			68.3	133.3
$\gamma + \not{E}$		0.2	0.2					2.8	0.1
All visible	110.9	33.2	40.4	33.7	33.3	88.7	39.4	1369	1097

($b\bar{b}+\not{E}$) signal. In scenario B, independently from Higgs bosons, the bulk of the total visible signal (which is about 105 fb) comes from the hadronic signature, mostly due to light quarks. Rather lower rates correspond to scenario C, where again most of the signal corresponds to hadronic final states. Even lower rates correspond to scenario D, where all the visible signal (about 45 fb) comes from charged lepton pairs. As for the single-photon signal, we find at most a few fb's in NR^+.

A less favorable situation is found for the neutralino region scenarios with $\tan\beta = 4$ (Table VI). Here, unless Higgs bosons are light enough to allow direct two-body decays, total visible rates never exceed 40 fb. For light Higgs bosons, one can reach, in scenario E, a total visible signal of about 111 fb.

As for the high cross-section regions, while the bulk of visible rates corresponds to two jets $+\not{E}$ signal, there are non-negligible rates even for more interesting signatures coming from cascade $\tilde{\chi}_2^0$ decays into charginos. For instance, in the H^+ scenario for $\tan\beta = 1.5$, one finds about 162 fb for the signal four jets $+\not{E}$ and about 109 fb (4×27.2) for the signal $e^{\pm}$ ($\mu^{\pm}$) $+ 2j + \not{E}$.

In the first phase of running at LEP 2, the c.m. energy will be slightly lower (i.e., $\sqrt{s} = 175$ GeV) than the one assumed here. Small differences are expected in this case. The general trend of variation can be inferred by comparing Fig. 17, at $\sqrt{s} = 190$ GeV, with Fig. 24, at $\sqrt{s} = 175$ GeV, for the visible cross section. On the one hand, there is a small reduction of the explorable region in the SUSY parameter space because of the smaller available phase space at $\sqrt{s} = 175$ GeV (cf. Fig. 13). As a consequence, one can observe that the relative importance of the neutralino region with respect to the chargino region is slightly increased. On the other hand, in HCS regions, where s-channel Z^0 exchange dominates, cross sections generally grow by about 20% at $\sqrt{s} = 175$ GeV.

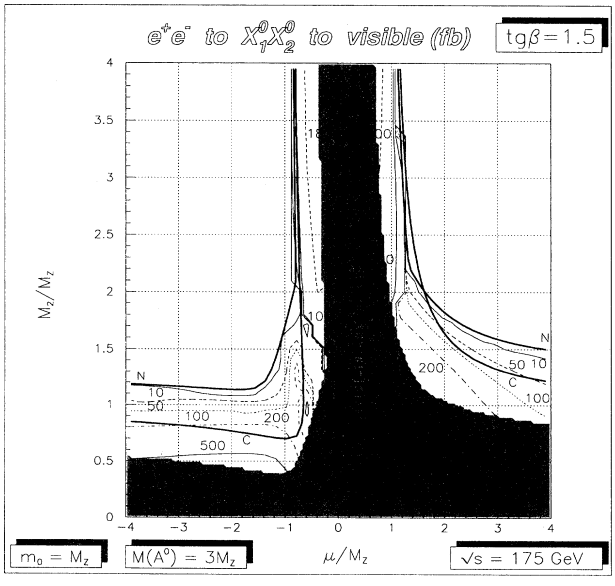

FIG. 24. Contour plot for the total rate (in fb) of visible events coming from $\tilde{\chi}_1^0\tilde{\chi}_2^0$ production at the first phase of LEP 2 ($\sqrt{s} = 175$ GeV).

In conclusion, we have found that neutralino production through the channel $e^+e^- \to \tilde{\chi}_1^0\tilde{\chi}_2^0$ can considerably extend the MSSM parameter space explorable at LEP 2. Although neutralino cross sections are comparable to chargino-pair production rates only in the high cross-section regions, where neutralinos are mostly Higgsinos, the most interesting parameter regions are what we named neutralino regions, where chargino-pair production is above threshold. In the neutralino regions, total rates for neutralino production crucially depend on selectron masses. Sizable rates are obtained mainly in the NR^- for $\tan\beta$ not too far from 1 and for $m_0 \lesssim 200$–300 GeV. Depending on the particular scenario selected in the parameter space, the best channel for neutralino detection can be either a leptonic or a hadronic one.

Of course, in order to fully assess the potential of neutralino searches as a tool to discover SUSY at LEP 2, a comparative study of the SM processes that can mimic the neutralino signal has to be performed. This will necessarily take into account also distributions of relevant kinematical variables, such as missing momenta and invariant mass of detected leptonic and hadronic systems.

ACKNOWLEDGMENTS

Interesting discussions with Guido Altarelli, Gian Giudice, Howie Haber, Stavros Katsanevas, and Fabio Zwirner are gratefully acknowledged.

APPENDIX

In this appendix we collect all relevant formulas we use to calculate sfermion- and Higgs-boson-mass spectrum in the framework of the MSSM with unification assumptions at the GUT scale. The neutralino and chargino sector of the model is treated in Sec. II.

For sfermion masses, once the value of m_0 is fixed at the GUT scale, one finds, by performing the RGE evolution down to the EW scale [21,22]

$$m^2_{\tilde{f}_{L,R}} = \tilde{m}^2_F + m^2_f \pm M^2_D, \tag{A1}$$

where $m_{\tilde{f}_{L,R}}$ is the mass of the generic sfermion $\tilde{f}_{L,R}$ and $\tilde{m}_F$, m_f are the corresponding evolved soft SUSY-breaking mass and fermion mass, respectively. We will name $\tilde{m}_{Q(L)}$ the soft mass for left squarks (sleptons) and $\tilde{m}_{U_R\cdots E_R}$ the soft masses for right squarks and charged leptons. In Eq. (A1), M^2_D is the so-called "D term,"

$$M^2_D = (T_{3,f_{L,R}} - Q_{f_{L,R}} \sin^2\theta_W) M^2_Z \cos 2\beta\ ,$$

where $T_{3,f}$ and Q_f are the $SU(2)_L$ and $U(1)_{em}$ (in units of $e > 0$) quantum numbers of the fermion f. For the soft masses of the first two generations, Yukawa-coupling effects can be neglected, and simple formulas hold. Indeed, they can be expressed, as functions of the scale Q and in terms of the common scalar and gaugino

masses m_0 and $m_{1/2}$ at the GUT scale $M_{\rm GUT}$ (where $\alpha_1(M_{\rm GUT}) = \alpha_2(M_{\rm GUT}) = \alpha_3(M_{\rm GUT}) = \alpha_{\rm GUT} \simeq \frac{1}{25}$), through the equations

$$\tilde{m}_L^2(t) = m_0^2 + m_{1/2}^2 \frac{\alpha_{\rm GUT}}{4\pi}\left[\frac{3}{2}f_2(t) + \frac{3}{10}f_1(t)\right], \quad \text{(A2a)}$$

$$\tilde{m}_{E_R}^2(t) = m_0^2 + m_{1/2}^2 \frac{\alpha_{\rm GUT}}{4\pi}\left[\frac{6}{5}f_1(t)\right], \quad \text{(A2b)}$$

$$\tilde{m}_Q^2(t) = m_0^2 + m_{1/2}^2 \frac{\alpha_{\rm GUT}}{4\pi}\left[\frac{8}{3}f_3(t) + \frac{3}{2}f_2(t) + \frac{1}{30}f_1(t)\right], \quad \text{(A2c)}$$

$$\tilde{m}_{U_R}^2(t) = m_0^2 + m_{1/2}^2 \frac{\alpha_{\rm GUT}}{4\pi}\left[\frac{8}{3}f_3(t) + \frac{8}{15}f_1(t)\right], \quad \text{(A2d)}$$

$$\tilde{m}_{D_R}^2(t) = m_0^2 + m_{1/2}^2 \frac{\alpha_{\rm GUT}}{4\pi}\left[\frac{8}{3}f_3(t) + \frac{2}{15}f_1(t)\right], \quad \text{(A2e)}$$

where $f_i(t)$ are RGE coefficients at the scale Q, given by

$$f_i(t) = \frac{1}{\beta_i}\left(1 - \frac{1}{(1+\beta_i t)^2}\right), \quad i = 1,2,3, \quad \text{(A3a)}$$

$$\beta_i = \frac{b_i}{4\pi}\alpha_{\rm GUT}, \quad i = 1,2,3, \quad \text{(A3b)}$$

$$t = \log\frac{M_{\rm GUT}^2}{Q^2}. \quad \text{(A3c)}$$

In Eq. (A3b), $b_{1,2,3}$ control the evolution of U(1), SU(2), and SU(3) gauge couplings at the one-loop level. Assuming for simplicity that the whole MSSM particle content contributes to the evolution from $Q \simeq M_Z$ up to $M_{\rm GUT}$, they are

$$b_i = \begin{pmatrix} b_1 \\ b_2 \\ b_3 \end{pmatrix} = \begin{pmatrix} 0 \\ -6 \\ -9 \end{pmatrix} + N_{\rm fam}\begin{pmatrix} 2 \\ 2 \\ 2 \end{pmatrix} + N_{\rm Higgs}\begin{pmatrix} 3/10 \\ 1/2 \\ 0 \end{pmatrix}, \quad \text{(A4)}$$

where $N_{\rm fam} = 3$ is the number of matter supermultiplets and $N_{\rm Higgs} = 2$ the number of Higgs doublets in the minimal SUSY. Since in the present analysis we use M_2 at the EW scale as an independent parameter in the gaugino sector, we need also the one-loop RGE relation

$$M_{1,2,3}(M_Z) = \frac{\alpha_{1,2,3}(M_Z)}{\alpha_{\rm GUT}} m_{1/2}$$
$$\Rightarrow M_3(M_Z) = \frac{\alpha_3(M_Z)}{\alpha_2(M_Z)} M_2(M_Z)$$
$$= \frac{\alpha_3(M_Z)}{\alpha_1(M_Z)} M_1(M_Z), \quad \text{(A5)}$$

which allows us to express $m_{1/2}$ in terms of M_2 in Eqs. (A2) and from which, in particular, Eq. (2.3) follows. In order to properly evaluate the sfermion spectrum through (A2), we adopt a recursive procedure (see, e.g., Refs. [1,23]). First, for any fixed values of m_0 and M_2, we calculate *zeroth order* sfermion masses $m_{\tilde{f}}^0$ for $Q = M_Z$; then we use these values as an input in Eqs. (A2) (i.e., with $Q = m_{\tilde{f}}^0$ in the corresponding equation for $\tilde{m}_F$), in order to get out the *first-order* masses, and so on. After a few iterations we obtain fast convergence. In this way, a sufficient agreement with more sophisticated SUSY-spectrum calculations (see, e.g., Ref. [1]) is found. In all our analysis, we neglect both Yukawa-coupling effects in diagonal soft masses and left-right mixing for the third generation of sfermions.

Concerning the SUSY-Higgs sector, starting from the two independent parameters m_{A^0} and $\tan\beta$, we calculate masses from the relations [24]

$$(m_{H^0,h^0})^2 = \frac{1}{2}\left[m_{A^0}^2 + M_Z^2 + \Delta\right] \pm \sqrt{\left[\left(m_{A^0}^2 - M_Z^2\right)\cos 2\beta + \Delta\right]^2 + \left(m_{A^0}^2 + M_Z^2\right)^2 \sin^2 2\beta},$$
$$m_{H^\pm}^2 = m_{A^0}^2 + M_W^2, \quad \text{(A6)}$$

where

$$\Delta = \frac{3}{8\pi^2}\frac{g^2 m_t^4}{M_W^2 \sin^2\beta}\ln\left(1 + \frac{m_{\tilde{t}}^2}{m_t^2}\right). \quad \text{(A6a)}$$

Equations (A6) take into account only the dominant contributions coming from top-quark/top-squark loops, and we use it under the further assumptions $m_{\tilde{t}_{L,R}} = m_{\tilde{u}_{L,R}}$ and no $\tilde{t}_L$-$\tilde{t}_R$ mixing. All the above simplifications allow us to avoid the introduction of other SUSY parameters as $A_{\rm GUT}$ [or $A_t(M_Z)$] and $B_{\rm GUT}$, without seriously affecting our results.

[1] G. L. Kane, C. Kolda, L. Roszkowski and J. D. Wells, Phys. Rev. D **49**, 6173 (1994); **50**, 3498 (1994).
[2] For a review and references see H.-P. Nilles, Phys. Rep. **110**, 1 (1984); R. Barbieri, Riv. Nuovo Cimento **11**, 1 (1988).
[3] H. E. Haber and G. L. Kane, Phys. Rep. **117**, 75 (1985).
[4] R. Barbieri, G. Gamberini, G. F. Giudice, and G. Ridolfi, Phys. Lett. B **195**, 500 (1987); J. Ellis, G. Ridolfi, and F. Zwirner, *ibid.* **237**, 423 (1990).
[5] A. Bartl, H. Fraas, W. Majerotto, Nucl. Phys. **B278**, 1 (1986); A. Bartl, W. Majerotto, and B. Mösslacher, in *Proceedings of the Joint International Lepton-Photon Symposium and Europhysics Conference on High Energy Physics*, Geneva, Switzerland, 1991, edited by S. Hegarty, K. Potter, and E. Quercigh (World Scientific, Singapore, 1992), Vol. 1, p. 357.
[6] D. A. Dicus and X. Tata, Phys. Rev. D **35**, 2110 (1987); M. Chen, C. Dionisi, M. Martinez, and X. Tata, Phys. Rep. **159**, 201 (1988); J. F. Grivaz *et al.*, in *Proceedings of the ECFA Workshop on LEP 200*, Aachen, Germany, 1986, edited by A. Böhm and W. Hoogland (CERN Report No. 87-08, Geneva, Switzerland, 1987), Vol. II, p. 380.
[7] S. Ambrosanio and B. Mele, Report No. ROME1-1095/95, hep-ph/9508237 (unpublished).
[8] J. Ellis and G. G. Ross, Phys. Lett. **117B**, 397 (1982).
[9] J. M. Frère and G. L. Kane, Nucl. Phys. **B223**, 331 (1983).
[10] A. Bartl, H. Fraas, W. Majerotto, and N. Oshimo, Phys. Rev. D **40**, 1594 (1989).
[11] S. T. Petcov, Phys. Lett. **139B**, 421 (1984); S. M. Bilenky, N. P. Nedelcheva, and S. T. Petcov, Nucl. Phys. **B247**, 61 (1984); J. Ellis, J. M. Frère, J. S. Hagelin, G. L. Kane, and S. T. Petcov, Phys. Lett. **132B**, 436 (1983).
[12] M. Carena and C. E. M. Wagner, Report No. CERN-TH.7320/94, and references therein.
[13] A. Bartl, H. Fraas, W. Majerotto, and B. Mösslacher, Z. Phys. C **55**, 257 (1992).
[14] A. B. Lahanas, K. Tamvakis, and N. D. Tracas, Phys. Lett. B **324**, 387 (1994).
[15] D. Pierce and A. Papadopoulos, Phys. Rev. D **50**, 565 (1994); Nucl. Phys. **B430**, 278 (1994).
[16] E. Reya, Phys. Lett. **133B**, 245 (1983); R. Arnowitt, A. H. Chamseddine, and P. Nath, *ibid.* **129B**, 445 (1983); D. Dicus, S. Nandi, W. Repko, and X. Tata, Phys. Rev. D **29**, 1317 (1984); **30**, 1112 (1984); P. Chiapetta, J. Soffer, P. Taxil, F. M. Renard, and P. Sorba, Nucl. Phys. **B262**, 495 (1985); J. Ellis, J. S. Hagelin, D. V. Nanopoulos, and M. Srednicki, Phys. Lett. **127B**, 233 (1983); V. Barger, R. W. Robinett, W. Y. Keung, and R. J. N. Phillips, *ibid.* **131B**, 372 (1983); G. Altarelli, B. Mele, and S. Petrarca, Nucl. Phys. **B245**, 215 (1984); S. Dawson, E. Eichten, and C. Quigg, Phys. Rev. D **31**, 1581 (1985).
[17] H. Komatsu and J. Kubo, Phys. Lett. **157B**, 90 (1985); Nucl. Phys. **B263**, 265 (1986); H. E. Haber, G. L. Kane, and M. Quirós, Phys. Lett. **160B**, 297 (1985); Nucl. Phys. **B273**, 333 (1986); H. E. Haber and D. Wyler, *ibid.* **B323**, 267 (1989).
[18] J. F. Gunion *et al.*, Int. J. Mod. Phys. A **4**, 1145 (1987); J .F. Gunion and H. E. Haber, Phys. Rev. D **37**, 2515 (1988).
[19] A. Bartl, H. Fraas, and W. Majerotto, Z. Phys. C **41**, 475 (1988); A. Bartl, W. Majerotto, B. Mösslacher, and N. Oshimo, *ibid.* **52**, 477 (1991); **52**, 677 (1991); A. Bartl, W. Majerotto, B. Mösslacher, N. Oshimo, and S. Stippel, Phys. Rev. D **43**, 2214 (1991).
[20] Particle Data Group, L. Montanet *et al.*, Phys. Rev. D **50**, 1173 (1994).
[21] L. E. Ibáñez and C. López, Nucl. Phys. **B233**, 511 (1984); L. E. Ibáñez, C. López, and C. Munoz, *ibid.* **B256**, 218 (1985); L. E. Ibáñez and G. G. Ross, in *Perspectives on Higgs Physics*, edited by G. L. Kane (World Scientific, Singapore, 1992), p. 229, and references therein.
[22] W. de Boer, Prog. Part. Nucl. Phys. **33**, 201 (1994); W. de Boer, R. Ehret, and D. I. Kazakov, Report No. IEKP-KA/94-05, hep-ph/9405342, 1994 (unpublished).
[23] V. Barger, M. S. Berger, and P. Ohmann, Phys. Rev. D **47**, 1093 (1993); **47**, 2038 (1993); V. Barger, M. S. Berger, P. Ohmann, and R. J. N. Phillips, Phys. Lett. B **314**, 351 (1993); V. Barger, M. S. Berger, and P. Ohmann, Phys. Rev. D **49**, 4908 (1994).
[24] H. E. Haber and R. Hempfling, Phys. Rev. Lett. **66**, 1815 (1991); Y. Okada, M. Yamaguchi, and T. Yanagida, Prog. Theor. Phys. **85**, 1 (1991); Phys. Lett. B **262**, 54 (1991); J. Ellis, G. Ridolfi, and F. Zwirner, *ibid.* **257**, 83 (1991); **262**, 477 (1991); R. Barbieri, M. Frigeni, and F. Caravaglios, *ibid.* **258**, 167 (1991); A. Yamada, *ibid.* **263**, 233 (1991).

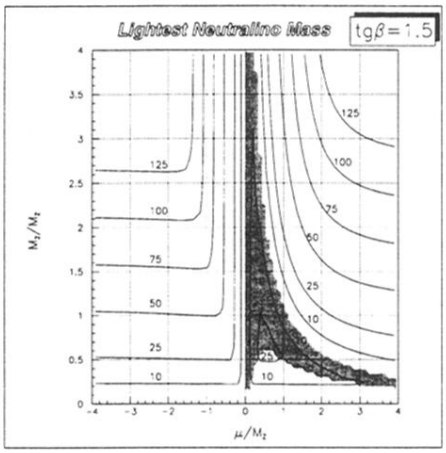

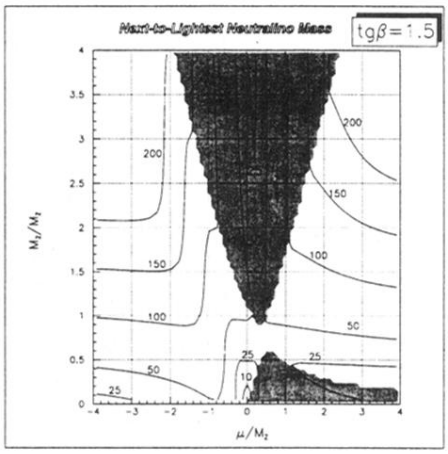

FIG. 6. Contour plot for the modulus of the LN and NLN mass eigenvalues (in GeV) in the (μ, M_2) plane for $\tan\beta$ =1.5. The dark area corresponds to regions where the $\tilde{\chi}^0_{1,2}$-mass eigenvalue is negative.